AGU PUBLICATIONS

JGR

Journal of Geophysical Research: Solid Earth

RESEARCH ARTICLE
10.1002/2017JB014769

Key Points:
- New southern North Atlantic (Iberia-North America) isochron map from Late Cretaceous to present
- Iberia was an independent plate from 83.5 to ~20.1 Ma, and the convergence between NW Africa and Iberia was active since 83.5 Ma
- Iberia-Europe convergence (Central Pyrenees) was NE directed from 83.5 to ~56 Ma, NW directed until ~46 Ma, and NNW directed till ~20.1 Ma

Supporting Information:
- Supporting Information S1
- Movie S1

Correspondence to:
C. Macchiavelli,
cmacchiavelli@ictja.csic.es

Citation:
Macchiavelli, C., Vergés, J., Schettino, A., Fernàndez, M., Turco, E., Casciello, E., … Tunini, L. (2017). A new southern North Atlantic isochron map: Insights into the drift of the Iberian plate since the Late Cretaceous. *Journal of Geophysical Research: Solid Earth*, *122*, 9603–9626. https://doi.org/10.1002/2017JB014769

Received 24 JUL 2017
Accepted 30 NOV 2017
Accepted article online 13 DEC 2017
Published online 29 DEC 2017

A New Southern North Atlantic Isochron Map: Insights Into the Drift of the Iberian Plate Since the Late Cretaceous

Chiara Macchiavelli[1], Jaume Vergés[1], Antonio Schettino[2], Manel Fernàndez[1], Eugenio Turco[2], Emilio Casciello[1], Montserrat Torne[1], Pietro Paolo Pierantoni[2], and Lavinia Tunini[1]

[1]Group of Dynamics of the Lithosphere, Institute of Earth Sciences Jaume Almera, ICTJA–CSIC, Barcelona, Spain, [2]School of Science and Technology-Geology Division, University of Camerino, Camerino, Italy

Abstract This paper presents a new southern North Atlantic plate model from Late Cretaceous to present, with the aim of constraining the kinematics of the Iberian plate during the last 83.5 Myr. This model is presented along with a detailed isochron map generated through the analysis of 3 aeromagnetic tracks and ~400 ship tracks from the National Centers for Environmental Information database. We present a new technique to obtain well-constrained estimates of the Iberia-North America plate motions from magnetic anomalies, overcoming the scarcity of large-offset fracture zones and transform faults. We build an integrated kinematic model for NW Africa, Morocco, Iberia, Europe, and North America, which shows that the deformation is partitioned between Pyrenees and Betic-Rif orogenic domain during the Late Cretaceous-Oligocene time interval. In the Eastern Betics domain, the calculated amount of NW Africa-Iberia convergence is ~80 km between 83.5 and 34 Ma, followed by ~150 km since the Oligocene. The motion of Iberia relative to Europe in the Central Pyrenees is characterized by overall NE directed transpressional motion during the Campanian and the Paleocene, followed by NW directed transpressional movement until the Lutetian and overall NNW directed convergence from Bartonian to Chattian. This motion occurs along the axis of the Bay of Biscay from the Santonian–Campanian boundary to the middle Priabonian, subsequently jumping to King's Trough at Anomaly 17 (36.62 Ma).

1. Introduction

The analysis of the specific behavior of small plates and the definition of the path of their displacement through time is one of the main goals of global kinematic reconstructions. Small plates can typically move independently from the large limiting plates and are often subject to large vertical axis rotations, as in the case of the Iberian plate. Iberia has been studied extensively since the 1980s through models describing the southern North Atlantic kinematics. These models were based on the analysis of marine magnetic anomalies and bathymetric or gravity data (DeMets et al., 2015; Kerr et al., 1981; Klitgord & Schouten, 1986; Merkouriev & DeMets, 2006, 2014a, 2014b; Miles & Kidd, 1986; Müller & Roest, 1992; Müller et al., 1990, 1997, 2016; Olivet et al., 1984; Olivet, 1996; Roest & Srivastava, 1991; Srivastava & Tapscott, 1986; Srivastava & Roest, 1989, 1992, 1996; Srivastava, Roest, et al., 1990; Srivastava, Schouten, et al., 1990; Srivastava et al., 2000; Sibuet & Collette, 1991; Sibuet, Srivastava, & Spakman, 2004; Sibuet, Monti, et al., 2004; Torsvik et al., 2001; Verhoef et al., 1996; Vogt, 1986) or on the reinterpretation of previously published data sets (e.g., rotation poles) to remove inconsistencies in the kinematic reconstructions (Rosenbaum, Lister, & Duboz, 2002; Vissers & Meijer, 2012a, 2012b). The seafloor spreading history of the southern North Atlantic between Iberia and Newfoundland and its relationship to the formation of the Pyrenees and Betic-Rif system (Figure 1) has been described involving successive jumps of the plate boundary between Iberia, Europe, and Africa from north (Bay of Biscay axis, B and King's Trough, KT; Figure 1) to south (Azores Gibraltar Fracture Zone, AGFZ; Figure 1) (Klitgord & Schouten, 1986; Olivet, 1996; Roest & Srivastava, 1991; Rosenbaum et al., 2002; Sibuet, Srivastava, & Spakman, 2004; Srivastava, Roest, et al., 1990; Srivastava, Schouten, et al., 1990; Vissers & Meijer, 2012a, 2012b).

Most of the plate-kinematic reconstructions of Iberia define two main kinematic phases: (i) a first phase associated with the opening of the Central Atlantic during the Jurassic-Cretaceous (154–83.5 Ma) and (ii) a second phase corresponding to Africa-Europe convergence since the Santonian-Campanian boundary (~83.5–0 Ma).

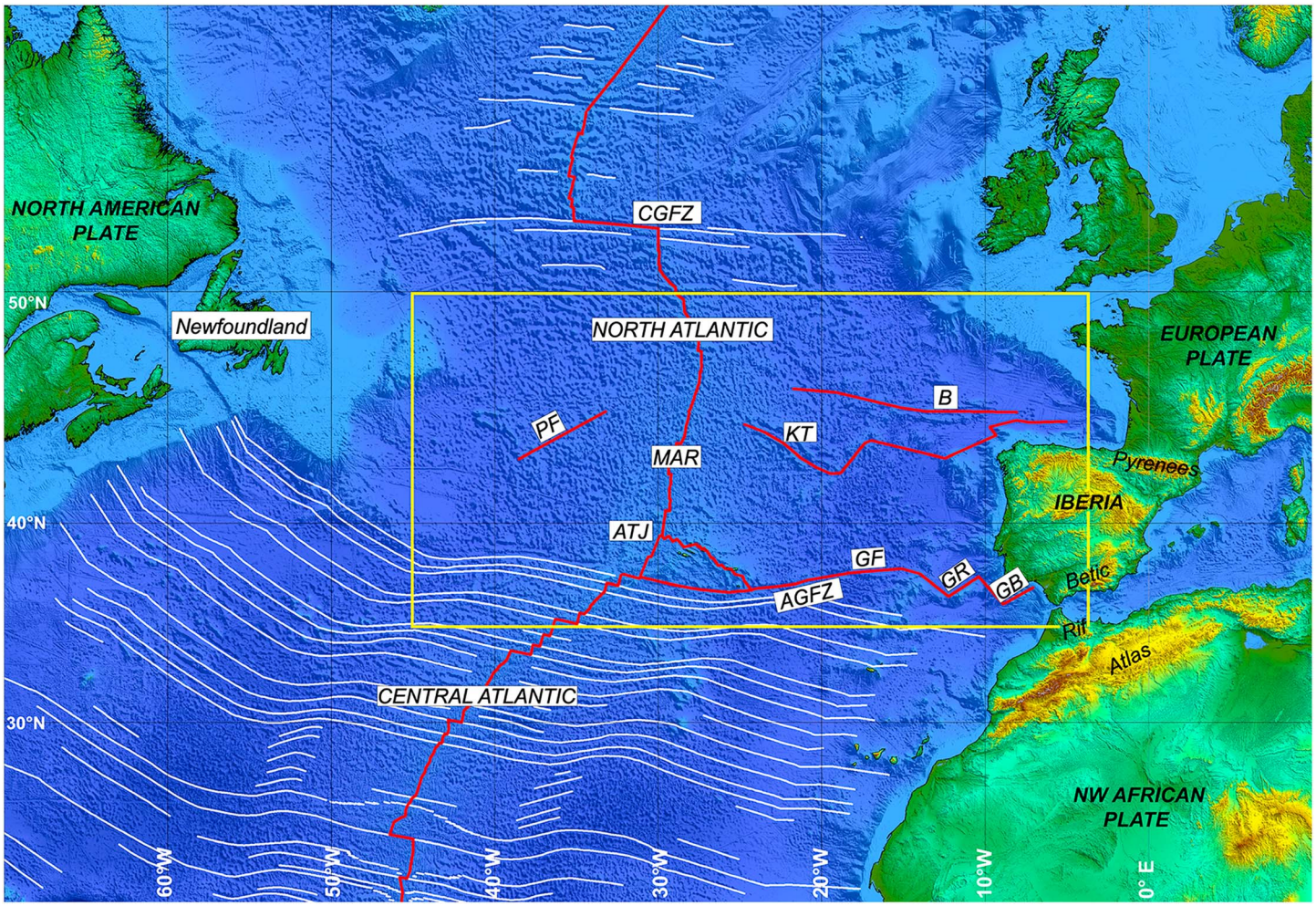

Figure 1. Topographic-bathymetric map of the southern North Atlantic. Red lines: plate boundaries; white lines: fracture zones; AGFZ: Azores Gibraltar FZ; ATJ: Azores Triple Junction; B: Bay of Biscay axis; CGFZ: Charlie Gibbs fracture zone; GB: Guadalquivir Bank; GF: Gloria Fault; GR: Gorringe Ridge; KT: King's Trough; MAR: mid-Atlantic ridge; PF: pseudo-fault, according to Srivastava and Roest (1992). The yellow box shows the location of the study area and where Figures 2, 4, 6, and 7 are featured.

The kinematics of Iberia during the first phase have been the subject of recent debate (Barnett-Moore et al., 2016; Bronner et al., 2011; Eddy et al., 2017; Nirrengarten et al., 2017; Norton et al., 2007; Péron-Pinvidic & Manatschal, 2009; Tucholke et al., 2007). Currently, three competing kinematic models have been proposed for the time interval from the Jurassic to the Cretaceous (154–83.5 Ma). The first model invokes a scissor-type opening of the Bay of Biscay (Sibuet, Srivastava, & Spakman, 2004; Sibuet, Monti, et al., 2004; Srivastava, Roest, et al., 1990; Srivastava, Schouten, et al., 1990; Srivastava et al., 2000; Vissers & Meijer, 2012a) and suggests up to 500 km of convergence across the Iberia-Europe plate boundary. The second model argues for dominant left-lateral strike-slip movement along the Iberia-Eurasia plate boundary (Handy et al., 2010; Le Pichon & Sibuet, 1971; Olivet, 1996; Stampfli et al., 2002). A third model requires transtensional motion along the Iberia-Europe plate boundary until the earliest Albian, with subsequent orthogonal extension between Iberia and Europe up to 83 Ma (Jammes et al., 2009).

For the second kinematic phase (83.5–0 Ma), most of the models show Iberia attached to Africa until the middle Eocene to middle Oligocene (Klitgord & Schouten, 1986; Olivet, 1996; Roest & Srivastava, 1991; Rosenbaum et al., 2002; Sibuet, Srivastava, & Spakman, 2004; Srivastava, Roest, et al., 1990; Srivastava, Schouten, et al., 1990). During this time span, the plate boundary between Africa and Europe was located along the northern boundary of the Iberian plate (B and KT-Pyrenees; Figure 1). From the late Oligocene to the present, Iberia was welded to the European plate, and as a result, the Africa-Europe plate boundary was located along the Iberian plate southern boundary (AGFZ-GR-GB-Betic-Rif system; Figure 1). However,

recent reviews of published rotation poles suggest an alternative reconstruction (Vissers & Meijer, 2012b) that allows for some 50–70 km of convergence between Africa and Iberia from the Late Cretaceous to the middle Eocene. Most of the kinematic models for the second phase follow a common approach to the calculation of rotation parameters for the Iberian plate. According to this procedure, Iberia is considered as part of Africa, and the relative motion along the boundaries is calculated from the differential motion between the Africa-North America and Europe-North America plate pairs (Klitgord & Schouten, 1986; Roest & Srivastava, 1991; Srivastava, Roest, et al., 1990; Srivastava, Schouten, et al., 1990). This approach has been widely used in kinematic models, because the limited length of the magnetic lineations and the poor-defined fracture zones prevent the determination of reliable reconstruction poles for North America and an independent Iberia plate. Srivastava, Roest, et al. (1990) obtained a good fit of North American and Iberian magnetic crossings by applying a correction pole P_a after rotating eastward North American magnetic crossings 34 (~83 Ma) to 18 (~39 Ma) with African poles of rotation. In addition, these authors observed that a second rotation about a pole, P_b, is required to obtain an adequate match for the magnetic crossings in the domain between King's Trough and the axis of the Bay of Biscay. On the basis of these observations, Srivastava, Schouten, et al. (1990) proposed a "jumping plate boundary" hypothesis in which the Europe-Africa boundary was located along the Bay of Biscay axis before jumping at Chrons 18–17 (Priabonian) to King's Trough and, finally, since Anomaly 6C (Chattian), to the Azores-Gibraltar Fracture Zone. In this view, pole P_a represents the total motion between Africa and Iberia along the Azores-Gibraltar Fracture Zone, whereas pole P_b reflects the total motion along King's Trough.

In this paper, we overcome the limitations related to the scarcity of fracture zones and the short length of the magnetic lineations by using a new iterative method that allows us to obtain an accurate and reliable rotation model without incorporating unreliable directional data. This method represents an evolution of techniques that have been used in the study of Red Sea kinematics (Chu & Gordon, 1998; Schettino et al., 2016). To better understand the kinematics of Iberia relative to NW Africa and Europe, we analyze 3 aeromagnetic tracks and ~400 ship-magnetic tracks of the National Oceanic and Atmospheric Administration National Centers for Environmental Information (NCEI) database (Figure S1 in the supporting information). We use this robust data set to determine magnetic anomaly picks of 37 magnetic anomalies located between the Azores Triple Junction (ATJ, ~39°N; Figure 1) and the axis of the Bay of Biscay (~46°N; Figure 1). First, we consider the area between the AGFZ and King's Trough as an independent plate from the Santonian-Campanian boundary (83.5 Ma) to the present. The resulting magnetic anomaly crossings are used to calculate North America-Iberia rotation parameters and to construct a new southern North Atlantic isochron chart. Then, through a comparison of the model-predicted lineations with the magnetic crossings, we test the "jumping plate boundary" hypothesis, formulate a new set of rotation poles for the study area, and propose a more detailed timing for the Iberia-Europe plate boundary jump. We use the data set thus constructed to build an integrated model of northwest Africa-Morocco-Iberia-Europe-North America plate motion, which allows for the shortening partitioning between Pyrenees and Betic domain related to the Africa-Europe convergence to be quantified. The proposed model is obtained combining our results with those published by Schettino and Turco (2011), Merkouriev and DeMets (2014a), and Schettino and Macchiavelli (2016). A set of plate reconstructions and convergence-rate diagrams illustrate the kinematics of the Iberian plate and show velocity fields across the major plate boundaries since the Santonian-Campanian boundary (83.5 Ma). To test our kinematic model in the Betic and Pyrenees orogenic system, we compare our shortening estimates with the temporal distribution of shortening implied by recent works (Beaumont et al., 2000; Mouthereau et al., 2014; and Vergés et al., 1995, for the Pyrenees and Vergés & Fernàndez, 2012, for the Betic domain). Moreover, we compare our results with previously published models using similar methodologies (Rosenbaum et al., 2002; Srivastava, Roest, et al., 1990; Srivastava, Schouten, et al., 1990; Vissers & Meijer, 2012b), with GPS data (Marques et al., 2013), and with a current plate motion model (DeMets et al., 2010). Finally, we present a short overview of the general mechanism controlling the southern North Atlantic and the Iberian kinematics.

2. Southern North Atlantic Magnetic Anomalies

From the 3 aeromagnetic tracks and the ~400 ship-magnetic tracks in the NCEI database for the southern North Atlantic, ~120 magnetic profiles have been extracted (Figure 2). The magnetic profiles were interpreted using *Magan* (Schettino, 2012), a software tool for the analysis of marine magnetic anomalies, the

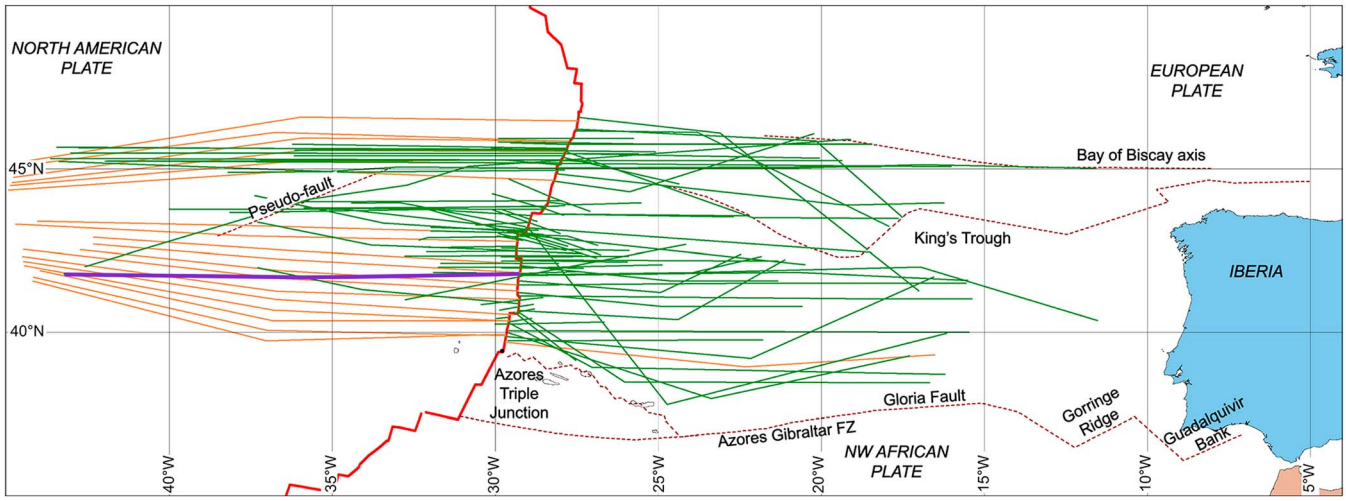

Figure 2. Tracks of magnetic (green lines) and aeromagnetic (orange lines) profiles used in this study. Thick purple line: location of the profile in Figure 3.

effectiveness of which has been demonstrated in other case-studies (e.g., Schettino et al., 2016; Schettino & Macchiavelli, 2016).

We identified crossing of 37 magnetic anomalies, between Anomaly 2A (2.58 Ma) and Anomaly 34 (83.5 Ma); the geomagnetic polarity time scale of Cande and Kent (1995) was used to assign the age of the correlation points (Figure 3). These points typically correspond to the young edge of the magnetic polarity interval. In only two cases, Anomalies 5 and 6, we assigned the correlation point to the main normal-reversed polarity chrons boundary (Müller et al., 1997). For Anomalies 21 and 33, we also considered the reversed polarity chron. The complete set of analyzed magnetic and aeromagnetic profiles is included in Figure S2 in the supporting information. The identified magnetic anomaly crossings are shown in Figure 4. Considering that the area between the AGFZ and King's Trough behaved as an independent plate from the Santonian-Campanian boundary (83.5 Ma) to the present, we calculate the finite Euler rotations of North America with respect to Iberia considering the crossings only from this area. It is worth noting that a limited area of the American side, between 40.5°N–43.3°N and 32.7°W–34.3°W (shaded area in Figure 4), has poor coverage of anomaly crossings. This area corresponds to a time interval between 24.73 Ma (Anomaly 7) and 34.55 Ma (Anomaly 15). For this time interval, it was not possible to obtain a realistic set of best fitting finite rotations. The Euler poles for Anomalies 2A–34 and the associated uncertainties were determined using the *PLACA* software (Matias et al., 2005), which includes an updated version of the Hellinger's algorithm (Hellinger, 1981). Each set of data (magnetic anomaly crossings and fracture zone sampling points) is assigned to one plate and is subdivided into different segments, so that the best fit pole results from the sum of segment contributions composed by independent sets of points. This model allows the best fit pole (three parameters: latitude, longitude, and angle of rotation) and the 2*N* parameters defining the *N* best great circles to be determined for each segment. The total number of degrees of freedom *F*, for *M* points and *N* segments, is

$$F = (M - 2) \times (N - 3).$$

The estimated errors for the magnetic crossing and for the fracture zones are the distances from each point to its great circle segment and to the predicted small circles parallel to the relative plate motion, respectively (Hellinger modified method; Matias et al., 2005). Although under special conditions (e.g., an excellent coverage of the magnetic crossings along the entire spreading ridge) it is possible to obtain well-constrained solutions using only magnetic anomaly crossings (Merkouriev & DeMets, 2008), fracture zones and transform faults represent important constraints for an accurate location of the reconstruction poles. Therefore, an accurate digitization of these lineaments, together with the determination of magnetic anomaly crossings, is required for a reliable estimation of rotation poles. Because in the southern North Atlantic a consistent set of fracture zones can be hardly determined, we reduced the significant uncertainty in the Euler pole determination using a method that represents an evolution of the techniques used by Schettino et al. (2016) to constraint the Red Sea kinematics. That method tried to overcome the scarcity of well-defined transform faults

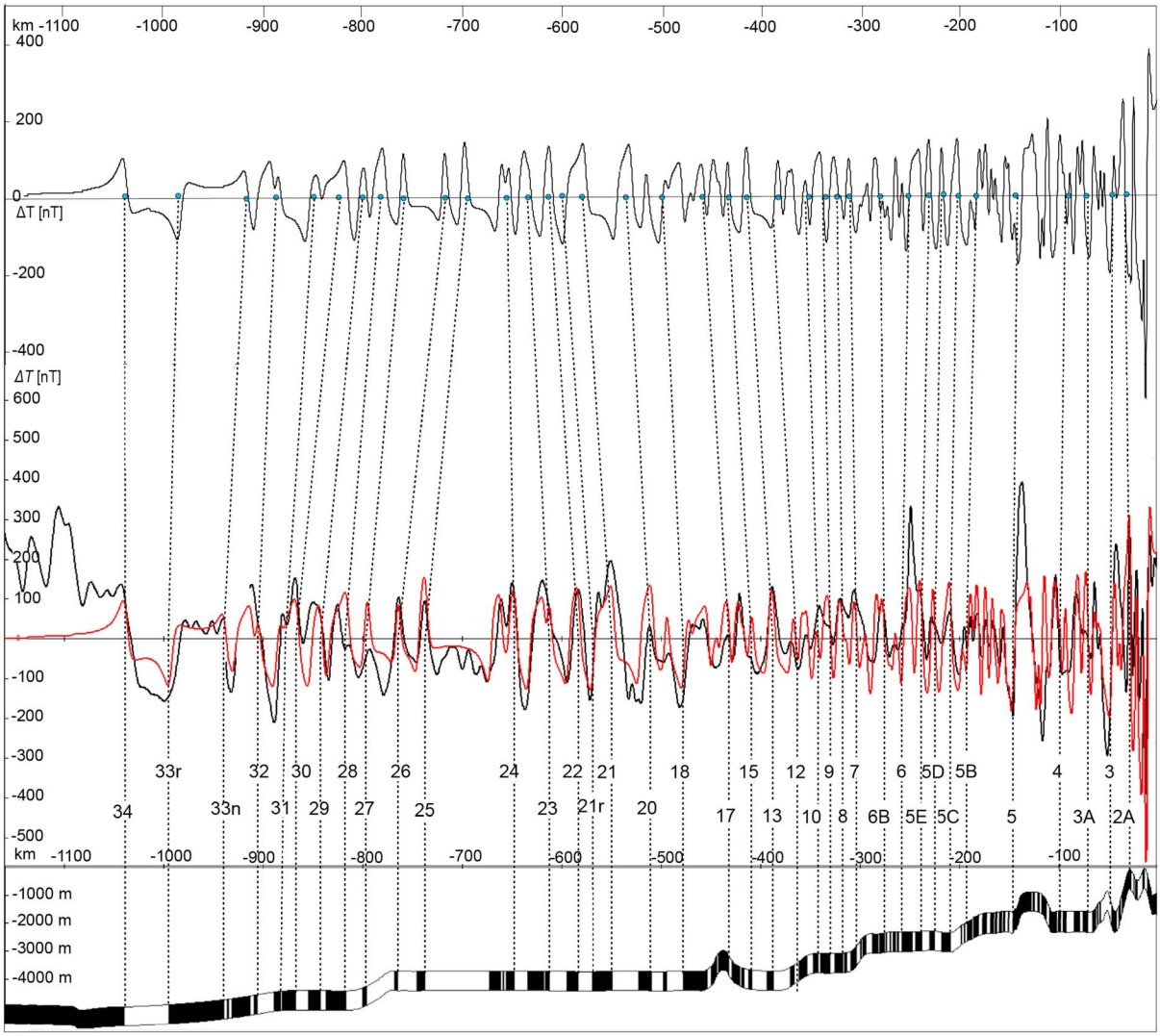

Figure 3. Correlation points for the 37 magnetic anomalies along the profile highlighted in Figure 2. (bottom) Best fitting magnetization model (black line). The numbers indicate anomaly locations along the magnetic profile. Red line: model anomalies. (top) Synthetic profile created for the average full spreading rate (26 mm yr^{-1}) of the best fitting magnetization model.

and fracture zones by integrating several sources of data. Synthetic lineaments were constructed "by interactively fitting sets of small circle arcs about test Euler poles to local kinematic indicators identified in the Red Sea and along the Arabian margin" (Schettino et al., 2016). However, in the present case study the kinematic indicators considered by Schettino et al. (2016) (e.g., local azimuth of synrift transcurrent fault or alignment of transform faults with continental strike-slip faults) could not be used, and therefore, a new approach was developed. We started using only magnetic anomaly crossings integrating them with synthetic fracture zones derived from the crossings themselves. Our approach can be described as an iterative procedure that starts from an initial solution based exclusively on a Hellinger statistic of magnetic crossings. At any step, a set of synthetic fracture zones is built, based on the current Euler pole. Points sampled along these fracture zones are then included in the Hellinger statistics to search for a new improved Euler pole. The procedure is repeated until a stable solution is found, which is not statistically distinguishable from the previous solution. The procedure is illustrated in Figure 5. At the initial step, we calculate Euler pole P_1, fitting only magnetic anomaly crossings (Figure 5a, blue dots). The large confidence ellipse (Figure 5a, purple ellipse e_1) shows that the exclusive use of magnetic anomaly crossings leads to a very poorly constrained solution (Matias et al., 2005; Srivastava, Roest, et al., 1990). However, directional data that are implicitly included in the original data set of conjugate crossings have not been used in this

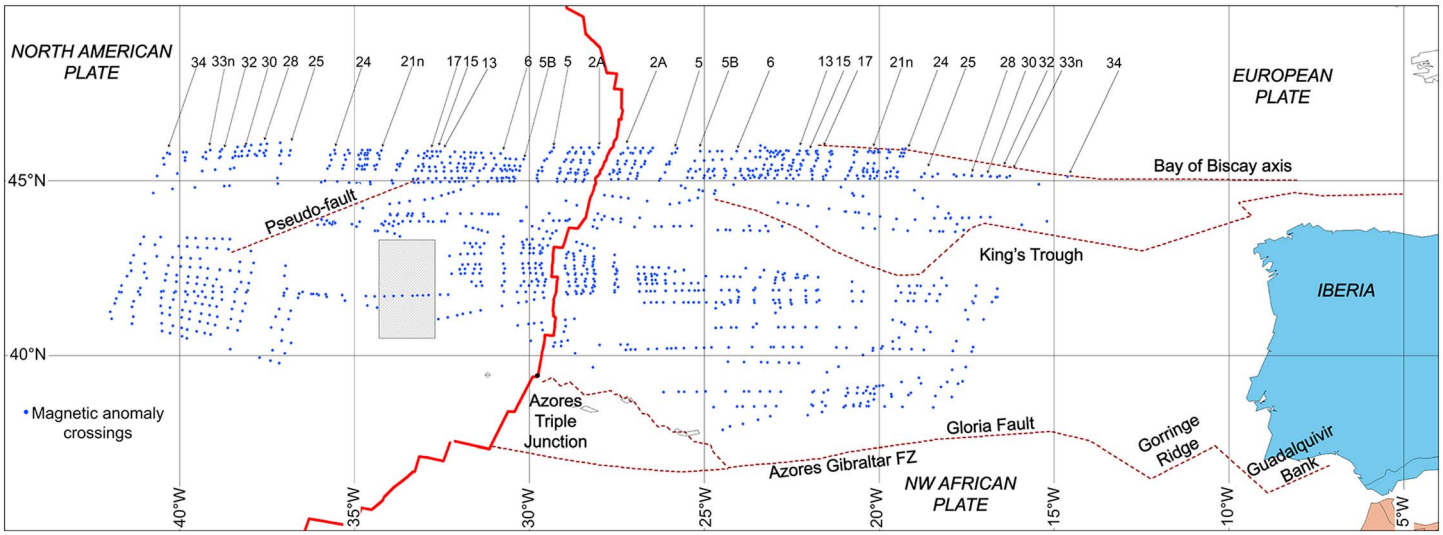

Figure 4. Identified magnetic anomaly crossings. Shaded area: lack of data zone.

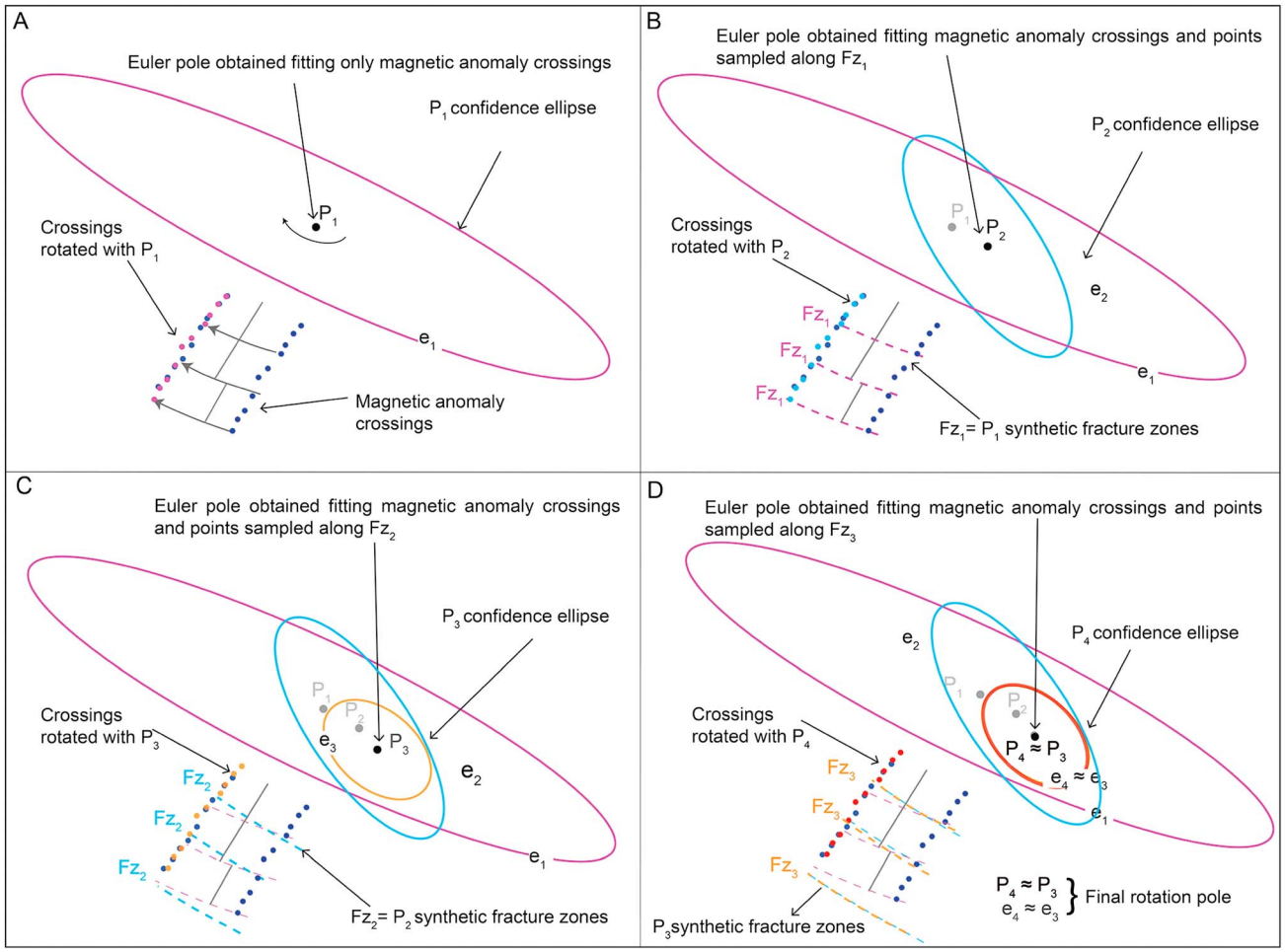

Figure 5. Iterative procedure used for finite reconstruction poles.

initial fit. Therefore, at the next step, we build a set of synthetic fracture zones (Figure 5b, purple dashed lines FZ_1) starting from the flow lines of the initial pole P_1 to supplement Hellinger's algorithm with directional data representative of hypothetical fracture zones and reduce the uncertainties in the rotation pole estimate. Using both magnetic anomaly crossings (Figure 5b, blue dots) and the synthetic fracture zones about P_1 (Figure 5b, purple dashed lines FZ_1), we obtain a second Euler pole (Figure 5b, P_2) and its associated confidence ellipse (Figure 5b, pale blue ellipse e_2). It is worth noting that this procedure will benefit from the use of real transform faults and fracture zones digitized on free-air gravity anomaly and bathymetric maps. The approach developed for the present case study is characterized by another level of arbitrariness related to the number of the synthetic fracture zones and fracture zone points. Since it is not possible to establish a priori what is the correct balance between the number of fracture zone points and the number of magnetic anomaly crossings, a trial and error procedure is needed. The creation of synthetic fracture zone sets eventually allows to introduce additional constraints to the Euler pole location without incorporating unreliable directional data. When the balancing is correct (i.e., bias is not introduced into the data set), the newly created Euler pole (P_2, Figure 5b) mostly falls inside the first confidence ellipse defining a new confidence ellipse (Figure 5b, pale blue ellipse e_2) smaller than the first one (e_1, Figure 5b). As a result, we can use Euler pole P_2 to construct the synthetic fracture-zone data set FZ_2 (Figure 5c, pale blue dashed line) and repeat the same procedure to obtain pole P_3 and confidence ellipse e_3 (Figure 5c). This procedure can be reiterated *n* times to generate a sequence of poles that converges toward a stable solution. As the number of iteration increases, the angular distance between Euler pole P_n and the previous pole (P_{n-1}) becomes smaller and the confidence regions tends to overlap (Figure 5d; the Euler poles P_3 and P_4 and their associated confidence ellipses e_3 and e_4 overlap). The reduction in size of the confidence ellipses and convergence occurs if the problem is well conditioned (i.e., if the number of the fracture-zone points does not exceed that of the magnetic crossings).

To test how robust is the method, we applied this procedure to a case study in the Central Atlantic (Schettino & Macchiavelli, 2016). To this purpose, we chose the set of magnetic crossings corresponding to Anomaly 12 (30.48 Ma), which provided a finite reconstruction pole E = 75.33°N, 0.66°E, 9.11°, when used in conjunction with real fracture zone data (Schettino & Macchiavelli, 2016), with a NE-SW elongated uncertainty ellipse (black square and pale blue ellipse in Figure S3 in the supporting information). At the first step, we obtained a rotation pole E_1 (Figure S3, gray dot) located at an angular distance from E of ~2.1°, albeit with a very large uncertainty ellipse (Figure S3, gray dotted line). Adding the E_1 synthetic fracture zones to the inversion procedure, the size of the uncertainty area was considerably reduced (red confidence ellipse 2 in Figure S3). The repetition of this procedure using the synthetic fracture zones obtained from poles E_2 to E_9 led to progressively smaller confidence ellipses and angular distance between the new calculated pole and the pole E (Figure S3). It is worth noting that the last criterion to validate each solution is its coherence in the framework of global rotation models. Especially in this context, in which the constraints offered by the magnetic crossings themselves are not particularly binding (e.g., the short length of the magnetic lineations), clearly, the best solution takes into account of the geological constraints founded on geologic criteria (e.g., consequences on the plate boundaries, such as in the Pyrenees, or in the Betic-Rif orogenic system).

The iterative method proposed in this study allowed us to obtain accurate Iberia-North America finite reconstruction poles and to reduce the error ellipses without incorporating unreliable directional data. The 1σ random noise in anomaly picking varies between 1.7 and 5.0 km. The total reconstruction poles associated with the iterative procedure described, along with degree of freedom *F*, 1σ uncertainty of the crossing position in the spreading direction, and covariance matrices (Matias et al., 2005), are listed in Table 1.

3. Isochron Charts and Iberia-North America Plate Motions

The reconstruction poles in Table 1 were used to reconstruct the magnetic anomaly crossings on the opposite sides of the ridge (Figure 6, red dots). As mentioned above, starting from Anomaly 7 (24.73 Ma) to Anomaly 15 (34.55 Ma), the lack of crossing points makes the statistical estimation of rotation parameters unreliable. However, we assumed a unique stage between 22.59 Ma (6B) and 36.62 Ma (17) and, by means of the best fit ting rotations (Table 1), calculated the stage pole of Iberia relative to North America at S = (85.05°N, 131.91°E) with a total angular displacement $\Delta\Omega = 3.172°$. Therefore, we obtained the predicted best fit reconstructions at each anomaly time (Anomalies 7, 8, 9, 10, 12, 13, and 15). The crossings and rotated crossings were used to build isochrons according to Schettino (2014).

Table 1
North America-Iberia Best Fitting Rotation

							Royer covariance matrices					
F	Anomaly	*Age* (Ma)	λ (deg)	φ (deg)	Ω (°deg]	δx (km)	C_1	C_2	C_3	C_4	C_5	C_6
43	2A	2.58	66.3	133.42	0.56	1.7	0.685	−1.191	0.004	5.181	−0.018	0.000
46	3	4.18	65.26	136.41	0.9	1.4	0.268	−0.852	0.005	4.032	−0.024	0.000
40	3A	5.89	63.75	137.4	1.25	2.0	0.260	−0.604	0.004	2.394	−0.018	0.000
22	4	7.43	64.22	135.91	1.6	2.2	0.425	−1.262	0.011	5.291	−0.046	0.001
33	5	10.95	65.32	135.24	2.53	3.0	0.313	−0.374	0.008	1.388	−0.025	0.001
30	5B	14.80	67.36	135.84	3.56	3.0	2.072	−3.272	0.156	0.156	−0.297	0.017
41	5C	16.01	67.78	135.93	3.87	2.9	0.045	−0.219	0.005	1.624	−0.034	0.001
28	5D	17.28	67.57	137.49	4.2	2.6	0.216	−0.930	0.024	4.571	−0.115	0.003
26	5E	18.28	67.51	137.82	4.45	2.6	0.511	−1.029	0.009	4.758	−0.037	0.002
27	6	20.13	67.6	139.51	4.94	2.4	0.031	−0.185	0.006	1.394	−0.045	0.002
15	6B	22.59	68.68	137.35	5.45	2.4	0.465	−1.581	0.110	7.032	−0.499	0.038
	7	24.73	69.99	137.05	5.91							
	8	25.82	70.59	136.9	6.1							
	9	27.03	71.2	136.8	6.4							
	10	28.28	71.8	136.59	6.69							
	12	30.48	72.7	136.3	7.17							
	13	33.06	73.6	136.01	7.75							
	15	34.55	74.05	135.85	8.06							
16	17	36.62	74.68	135.61	8.54	4.1	0.132	−0.481	0.037	2.272	−0.174	0.014
18	18	38.43	74.98	134.57	8.99	4.1	0.406	−0.840	0.040	5.090	−0.228	0.015
16	20	42.54	76.02	133.2	10.02	3.0	1.312	−2.679	0.357	6.293	−0.830	0.117
18	21n	46.26	76.56	131.72	11.00	2.3	0.636	−0.691	0.146	0.871	−0.175	0.038
21	21r	47.90	77.13	130.01	11.39	2.2	0.167	−0.445	0.067	4.087	−0.722	0.137
20	22	49.04	77.09	130.53	11.88	2.4	0.511	−1.029	0.009	4.758	−0.037	0.002
22	23	50.78	77.03	130.75	12.5	3.0	2.310	−4.130	0.679	7.783	−1.267	0.211
22	24	52.36	76.98	131.95	13.05	3.0	0.045	−0.219	0.005	1.624	−0.034	0.001
22	25	55.90	77.01	133.06	14.6	3.4	1.358	−2.242	0.376	7.619	−1.176	0.220
20	26	57.55	76.90	134.17	15.12	3.3	0.210	−0.439	0.083	0.979	−0.185	0.039
24	27	60.92	76.74	136.45	15.99	5.0	0.103	−0.311	0.050	1.329	−0.223	0.039
22	28	62.50	76.68	137.56	16.39	3.0	0.065	−0.239	0.054	0.982	−0.227	0.053
23	29	63.98	76.85	138.04	16.74	4.2	0.093	−0.503	0.089	2.984	−0.533	0.096
26	30	65.58	77.02	138.54	17.11	4.7	0.177	−0.445	0.062	4.091	−0.718	0.136
23	31	67.74	77.25	139.21	17.62	3.9	0.015	−0.126	0.020	2.240	−0.368	0.061
22	32	71.07	77.75	140.77	18.35	3.6	0.007	−0.036	0.005	1.055	−0.172	0.028
23	33n	73.62	78.71	141.11	19.1	4.2	0.011	−0.106	0.025	2.461	−0.585	0.140
23	33r	79.08	80.52	141.94	20.95	4.9	0.453	−0.139	0.029	5.529	−1.083	0.010
21	34	83.50	81.81	143.29	22.27	2.5	0.033	−0.013	−0.003	1.894	−0.191	0.025

Note. *F*: degrees of freedom: M-2*N-3 (M: number of fracture-zone and anomaly points; N: number of fracture-zone and anomaly segments). λ: latitude; φ: longitude; Ω: rotation angle (ccw positive); δx: 1σ uncertainty of the crossing position in the spreading direction; C_1, C_4, and C_6: diagonal components of the variance-covariance matrix; C_2, C_3, and C_5: off-diagonal elements.

Figure 7a shows the new isochron map for the southern North Atlantic area since Anomaly 34. This chart gives a clear view of the ridge processes from 83.5 Ma to present. For instance, we observe that three ridge segments coalesce in a unique segment after Anomaly 4 (7.43 Ma) and after Anomaly 24 (52.36 Ma) (Figure S4a in the supporting information).

We also detect the presence of small fracture zones (maximum offset ~30 km) from Anomaly 2A to Anomaly 5 at ~43.5°N and from Anomaly 2A to 18 at ~40.5°N (Figure S4a). Multiple episodes of pseudo-fracture-zone formation can be identified, all related to variations in spreading asymmetry. The ridge geometry remains relatively constant from Anomaly 5B (14.80 Ma) to Anomaly 18 (38.43 Ma) and from Anomaly 26 (57.55 Ma) to Anomaly 31 (67.74 Ma). Conversely, the ridge geometry is characterized by a continuous reorganization from Anomaly 20 (42.54 Ma) to Anomaly 24 (52.36 Ma) with a progressive northward migration of the pseudo-fracture zone located at ~40.5°N (Figure S4a).

Following Schettino and Macchiavelli (2016), to use our rotation parameters to predict and to compare local spreading rates with kinematic models of current plate motions or GPS data in the southern North Atlantic,

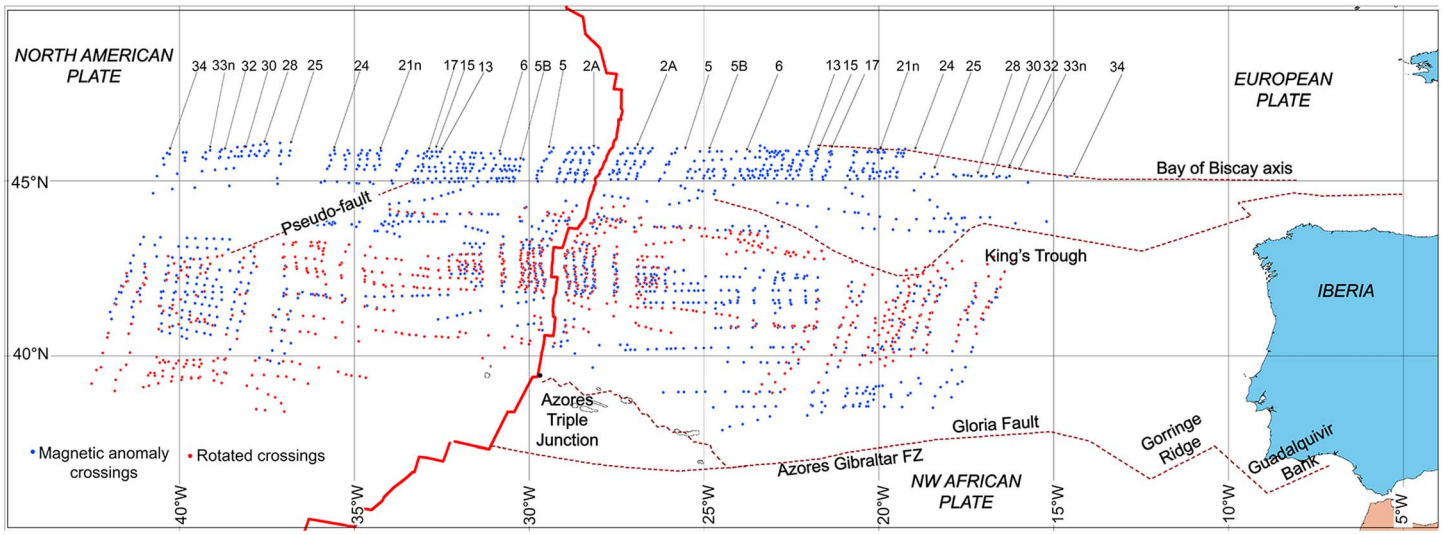

Figure 6. Crossings and crossings rotated using the reconstruction poles in Table 1.

we corrected our data both outward displacement (DeMets & Wilson, 2008) and we calculated the spreading asymmetry. The correction for outward displacement (DeMets & Wilson, 2008) was performed by applying to the 2A pole in Table 1 an angular correction of $\Delta\Omega = 0.0118°$ (see Schettino & Macchiavelli, 2016). Therefore, we obtain a linear distance spanning from 1.19 km at ~46°N to 1.25 km at ~39°N, in accordance with the results of DeMets and Wilson (2008), who reported outward displacement of 1–2 km for the ridge segments north of the ATJ. The overall spreading asymmetry since Anomaly 34 (83.5 Ma) ranges from ~4% to ~ −2%; between Anomalies 21 (46.26 Ma) and 34 (83.5 Ma) it ranges from ~9% to −2% (Table 2).

The detailed computation of the rotation parameters for the AGFZ-King's Trough area has been revealed to be a crucial tool for testing the "jumping plate boundary" hypothesis (Srivastava, Roest, et al., 1990; Srivastava, Schouten, et al., 1990) and to define a more precise timing of the plate boundary shift from the Bay of Biscay axis to King's Trough. In this area, we traced only representative magnetic lineations (Figures 7b and S4b, dashed lines) interpolating crossings and checked the fit between these magnetic crossings and the corresponding rotated crossings (Figures 7b and S4b, black dots), relative to the poles listed in Table 1. An important feature of these rotated crossings is the systematic mismatch with corresponding conjugate magnetic lineations. This mismatch ranges from a few kilometers for the younger anomalies (e.g., Anomaly 6r) to 30–40 km for the oldest anomalies. An excellent fit is obtained by rotating the younger anomalies (Anomalies 2A to 15; Figures 7c and S4c, green dots) with the Europe-North America rotation poles (Merkouriev & DeMets, 2014a; Rowley & Lottes, 1988). Conversely, these rotation poles did not provide a good match for the older anomalies. To obtain a satisfactory match (Figures 7c and S4c, red dots) for the magnetic crossings older than (and including) Anomaly 17 (36.62 Ma), it was necessary to apply an extra rotation of −1.026° to the Iberia-North America rotation poles about a pole P* located at 28.62°N, 34.64°W. These results confirm the "jumping plate boundary" hypothesis (Srivastava, Roest, et al., 1990; Srivastava, Schouten, et al., 1990) and define the exact time interval that the process occurred, around Anomaly 17 (36.62 Ma, Priabonian). From Anomaly 34 (83.5 Ma, Santonian-Campanian boundary) to Anomaly 17 (36.62 Ma), the Bay of Biscay-King's Trough area was part of an independent Iberian plate. From that time, all these anomalies started to move with Europe, and the correction pole P* corresponds to the differential motion between Iberia and Europe (an estimate of the total relative motion between Iberia and Europe along the King's Trough boundary) from Anomaly 17 (36.62 Ma) to the present.

The confidence ellipses for the best fitting rotations in Table 1 are shown in Figure 8a. We note that on a statistical basis, all the time intervals are distinct stages. We also note that there are different arrangements of Euler pole locations. The interval C2A–C6B is included between 60°N–70°N and 130°E–140°E; the Euler poles associated to Anomalies 17 to 21r are organized in a regular pattern directed nearly westward. On the contrary, the Euler pole locations at Anomalies 25 to 34 form an organized pattern directed toward east. It is important to point out that there is no kinematic information in this pattern of finite reconstruction poles

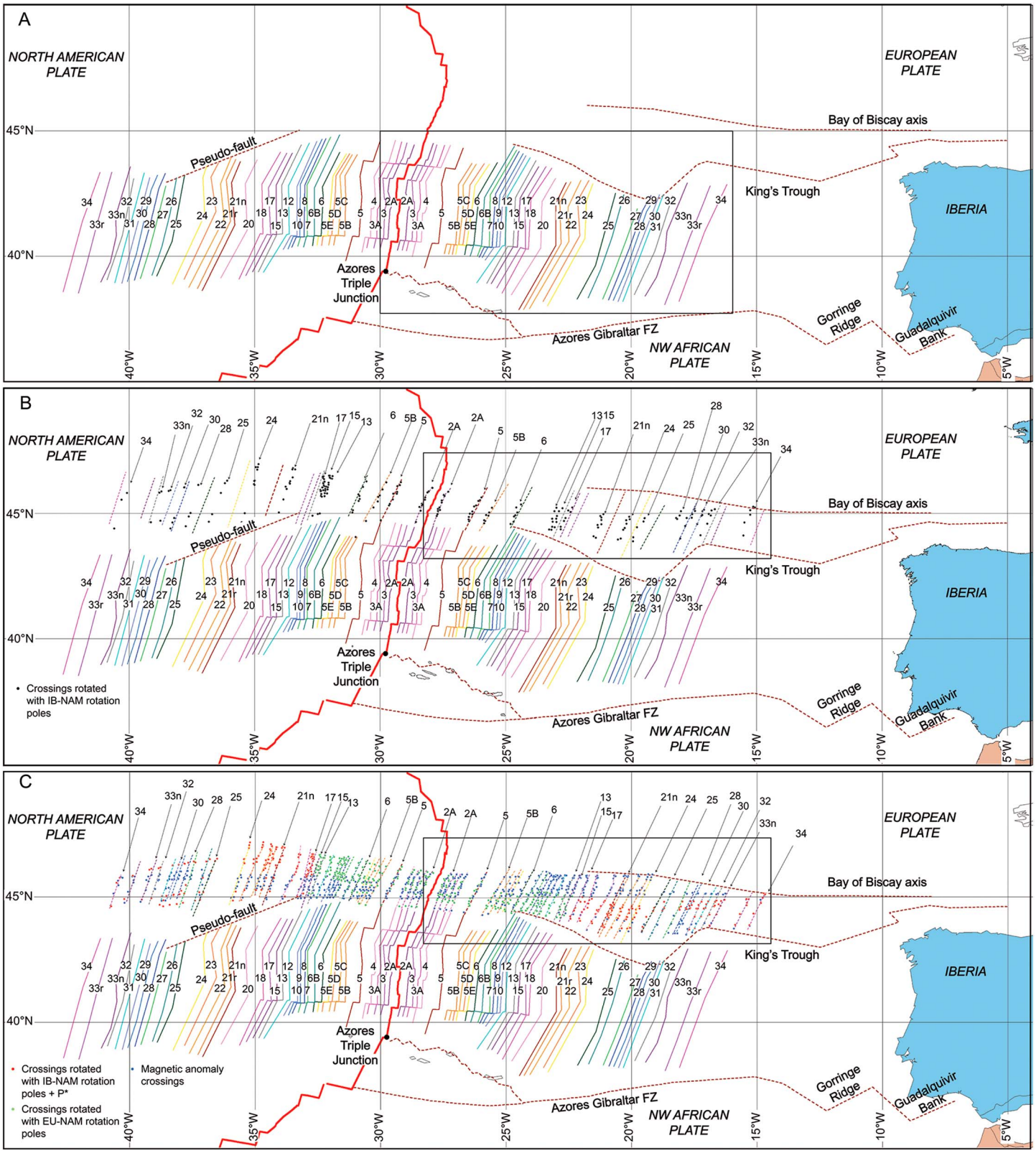

Figure 7. (a) Isochron chart of the southern North Atlantic region. The black box shows where Figure S4a is featured. (b) Systematic misfit of reconstructed magnetic crossings (Anomalies 2A, 5r, 5B, 6r, 13, 15, 17, 21n, 24, 25, 28, 30, 33n, and 34) with the corresponding magnetic lineation (dashed lines). The black box shows where Figure S4b is featured. (c) Corrected rotated magnetic crossings compared with the corresponding magnetic lineations (dashed lines). The black box shows where Figure S4c is featured.

Table 2
North America-Iberia Spreading Asymmetry (AGFZ-KT Area)

Δx_I An34 (km)	Δx_I An21n-An34 (km)	No.	λ (deg)	α An34 (%)	α An21n-An34 (%)
1060	528	1	42.97	4.2	8.8
1027	504	2	42.01	0.7	4.0
1016	488	3	40.82	−2.4	−2.2

Note. Δx_I An34: offset of Anomaly 34 calculated along a synthetic flow line from the Iberian side of the ridge (km); Δx_I An21n-An34: distance between anomalies 21n and 34 along a synthetic flow line from the Iberian side of the ridge (km); No.: segment number; λ: latitude of the intersection between the flow line and the ridge; α An34: overall spreading asymmetry since Anomaly 34; α An21n-An34: spreading asymmetry between anomalies 21n and 34.

(e.g., Schettino & Macchiavelli, 2016). This map only displays the position of the Euler pole obtained by the statistical analysis described in the sections above. More relevant is the information shown in Figures 8b and 8c. Figure 8b displays a plot of the average spreading rates along the southern North Atlantic ridge (red line), in which we observe significant changes at Anomalies 33r (79.08 Ma), 33n (73.62 Ma), 28 (62.50 Ma), 26 (57.55 Ma), 25 (55.90 Ma), 24 (52.36 Ma), 21r (47.90 Ma), 6 (20.13 Ma), and 4 (7.43 Ma). The path of the stage pole (Figure 8c) suggests that the time interval between Anomalies 28 (62.50 Ma) and 31 (67.74 Ma) is a single stage. However, the sharp velocity transition at Anomaly 28 (62.50 Ma) (Figure 8b) highlights that only Anomalies 29–31 form a single stage. Similarly, the sharp velocity transitions between Anomalies 26 (57.55 Ma) and 28 (62.50 Ma) and between Anomalies 32 (71.07 Ma) and 33r (79.08 Ma) reveal that they cannot be considered as a single stage, although the stage poles are very close (Figure 8c).

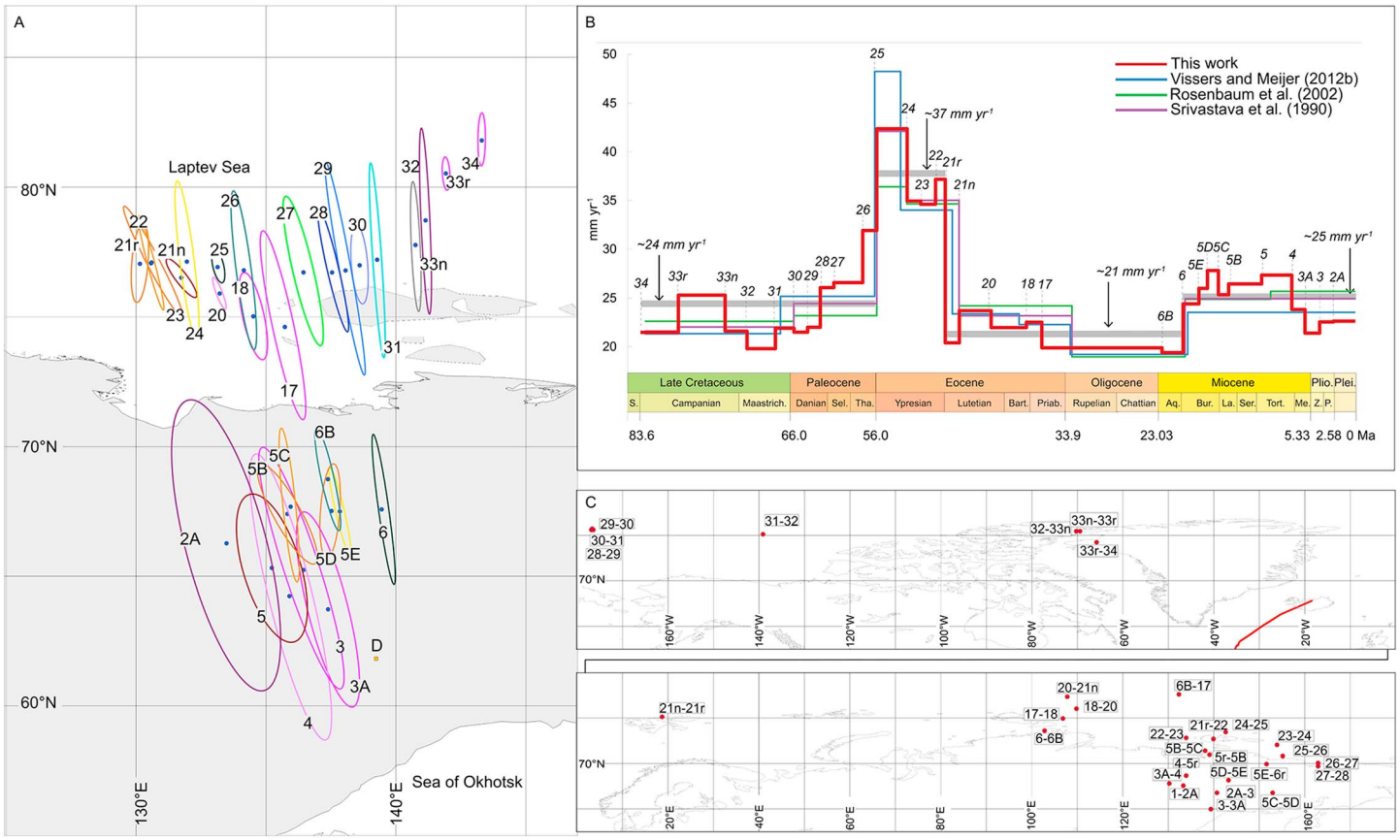

Figure 8. (a) Confidence ellipses for anomalies from 2A to 34. Orange square "D": 3.16 Myr average MORVEL Eurasia-North America rotation pole (DeMets et al., 2010). (b) Comparison of North America-Iberia spreading rates since Anomaly 34 (83.5 Ma) along the MAR in the King's Trough-Azores Gibraltar Fracture Zone area. The labels are magnetic anomaly timescale numbers. Thick gray line: average spreading rate (this study). (c) Location of North America-Iberia stage poles since Anomaly 34. (top) 55°N–90°N, 180°W–0°E; (bottom) 55°N–90°N, 0°E–180°E.

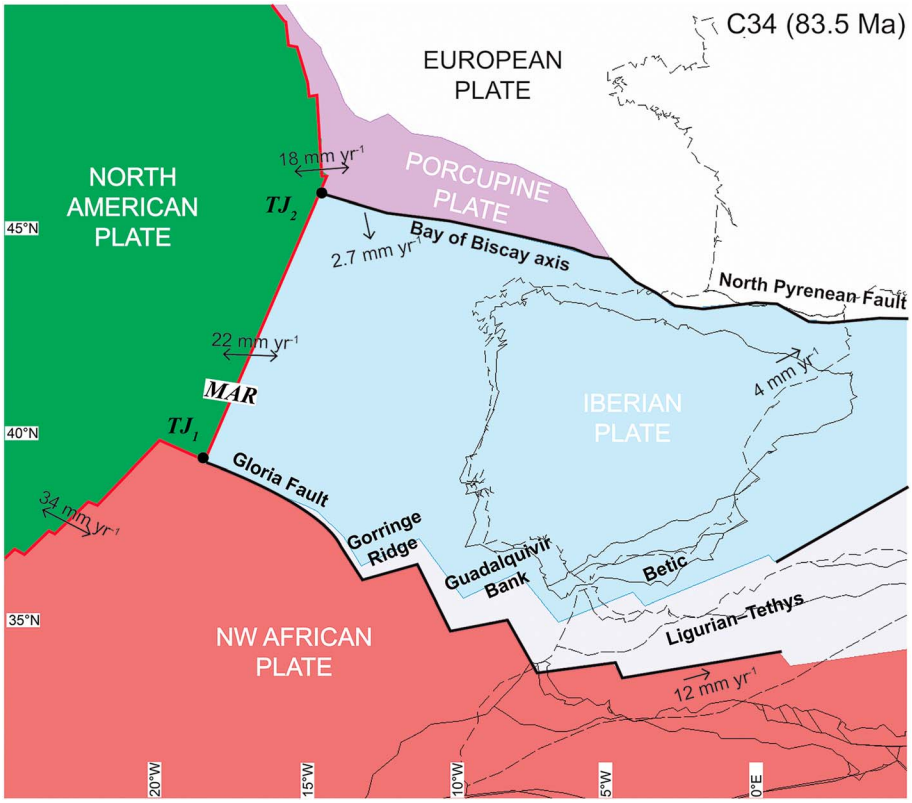

Figure 9. Iberia and surrounding plates at Chron 34. TJ_1: North America-Africa-Iberia triple junction; TJ_2: Europe (Porcupine) -North America-Iberia triple junction; MAR: Mid-Atlantic Ridge; black arrows with numbers: relative velocity vectors; black lines: plate boundaries. Present-day coastlines (dashed lines) are shown for reference.

4. Plate Reconstructions Since the Late Cretaceous (83.5 Ma)

The motion of the Iberian plate is strictly related to the seafloor-spreading history of the southern North Atlantic, as described above. This history cannot be separated from the kinematic restoration of the other surrounding plates (the European, Porcupine (the oceanic part of the European plate), North American, NW African, and Moroccan plates; Figure 9).

4.1. NW Africa-Iberia Plate Boundary

The opening of the Central Atlantic during the Early Jurassic determined the eastward movement of Africa with respect to Iberia (i.e., Europe), generating the Ligurian-Tethys domain, which was formed by several transtensive, highly extended rift basins. During that time, the kinematics of the Atlantic region was transferred to the Tethyan region through the preexisting plate boundary between Morocco and Iberia, namely, the Atlas and Betic Rift (Schettino & Turco, 2011). In our kinematic model, we retain the segmented characteristic of the Jurassic plate boundary already defined by previous authors (e.g., Frizon de Lamotte et al., 2011; Handy et al., 2010; Sallarès et al., 2011; Schettino & Turco, 2011; Vergés & Fernàndez, 2012), although with a slightly different geometry. Novelly, we consider three WNW-ESE oriented segments (Figure 9): the Gorringe Ridge, the Guadalquivir Bank, and the Betic segment. Since these proposed segments are the remnants of the Jurassic-Cretaceous plate boundary, they may not coincide with the present boundary that is still under reorganization (e.g., Deverchere et al., 2005; Zitellini et al., 2009). West of the Gorringe Ridge, the plate boundary continues along the Gloria Fault and intersects the MAR at triple junction TJ_1.

4.2. Iberia-Europe Plate Boundary

Seafloor spreading gradually propagated from the Central to the North Atlantic in several phases starting from the Iberia-Newfoundland and Porcupine-North America rifting phase. The Iberia-Newfoundland margin is a highly extended, magma-poor rifted continental margin (Péron-Pinvidic et al., 2007, and references

therein), and it underwent two main phases of extension lasting from the Late Triassic to Early Jurassic and from the Late Jurassic to Early Cretaceous (Tucholke et al., 2007). The location and onset of seafloor spreading are still questioned. Several studies suggest ages around anomalies M3–M5 (~124–128 Ma) (Russell & Whitmarsh, 2003; Whitmarsh & Miles, 1995) and late Aptian (~112–118 Ma) (Bronner et al., 2011; Eddy et al., 2017; Tucholke et al., 2007), respectively. Other studies suggest an older age (Anomaly M21, ~147 Ma) (Sibuet et al., 2007; Srivastava et al., 2000). During the Early Cretaceous, the counterclockwise motion of Iberia with respect to Europe triggered the opening of the Bay of Biscay (Sibuet, Srivastava, & Spakman, 2004; Sibuet, Monti, et al., 2004, and references therein) at a ridge-ridge-ridge (RRR) triple junction (Klitgord & Schouten, 1986). In our model, we defined the plate boundary between Iberia and Europe from the MAR (RRR triple junction TJ_2; Figure 9) along the Bay of Biscay axis up to the North Pyrenean Fault (Figure 9). The North Pyrenean Fault "has been commonly interpreted as a transform fault associated with a huge counterclockwise transverse and rotational movement that allowed the opening of the Bay of Biscay and the relative eastward motion of Iberia during the Mesozoic" (Canérot, 2016). Although the boundary between Iberia and Europe is a wide deformation zone (Canérot, 2016), in this study we used the North Pyrenean Fault as a representative boundary. The axis of the Bay of Biscay is linked to the North Pyrenean Fault through a NNW-SSE oriented transfer fault.

4.3. Porcupine Plate

Another piece of the puzzle for reconstructing Iberian kinematics is the Porcupine plate (Figure 9). The existence of an independent Porcupine plate was first postulated by Srivastava and Tapscott (1986), who noted that the Europe-North America rotation poles led to overlaps of Anomalies 21 and 24 in the area south of the Charlie Gibbs Fracture Zone (CGFZ) (Figure 1). In addition, those authors observed that the deformation occurred along the Porcupine and northern Biscay margins between ~56 and ~33 Ma cannot be explained by a single pole of rotation (Srivastava & Tapscott, 1986). Subsequently, Srivastava and Roest (1996) refined this concept and showed that this poor fit affected all the pre-Chron 13 (33.1 Ma, Rupelian) magnetic anomalies south of the CGFZ. Moreover, those authors emphasized that a single pole of rotation overcomes the mismatch between all magnetic lineations between Chrons 34 and 18. We used the Porcupine-Europe rotation of Srivastava and Roest (1996) from Anomaly 34 (83.5 Ma) to Anomaly 18 (38.43 Ma).

4.4. Plate Tectonic Evolution of the Southern North Atlantic

The motion of the Iberian plate since the Santonian-Campanian boundary (Chron C34, 83.5 Ma) is determined based on the estimated finite reconstruction poles listed in Table 1. The remaining rotations (Europe-North America, NW Africa-North America, and Morocco-NW Africa) can be found in Merkouriev and DeMets (2014a), Schettino and Scotese (2005, and references therein), Schettino and Turco (2011, and references therein), and in Schettino and Macchiavelli (2016). The plate tectonic evolution of the southern North Atlantic and surrounding plates relative to a fixed Europe is illustrated through a set of plate reconstructions at selected anomaly times (Figures 10 and 11). In each reconstruction, both active and abandoned plate boundaries are shown, along with triple junctions and velocity fields at the active boundaries. A reconstruction movie can be found in the supporting information. For the sake of simplicity, the plate reconstructions in Figures 10 and 11 are shown with present-day coastline configurations; the involved plates are considered to be internally rigid, and the inferred deformation is transferred along the plate boundaries, although it is only an approximation. However, a detailed analysis of the internal plate deformation is beyond the scope of the present study. At the Santonian-Campanian boundary (Chron C34, 83.5 Ma), a NW-SE directed extensional motion (~10 mm yr^{-1}) at the ATJ and along the Gloria Fault characterized the NW Africa-Iberia boundary. This motion became mainly ENE directed with an increased rate (up to ~12.0 mm yr^{-1}) in the Betic domain (Figure 10a). During the Campanian and the Maastrichtian, the NW Africa-Iberia velocity vectors gradually rotated counterclockwise, becoming N directed (~5–6 mm yr^{-1}) in the Betic domain (Figure 10b). The motion between Iberia and Europe was accommodated along the axis of the Bay of Biscay and along the North Pyrenean Fault, with this motion being mainly extensional in a NW-SE direction in the Bay of Biscay (Iberia-Porcupine boundary). The Iberia-Europe relative velocity vector progressively increased in magnitude up to ~4.0 mm yr^{-1} and rotated counterclockwise, becoming ENE directed up to the eastern tip of the North Pyrenean Fault (Figures 10a and 10b). According to our reconstruction, Africa almost stopped moving relative to Europe during the Paleocene (Schettino & Turco, 2011), and a small amount of extension (~25 km) is predicted among NW Africa, Iberia, and Europe. Most of the predicted extension was accommodated between

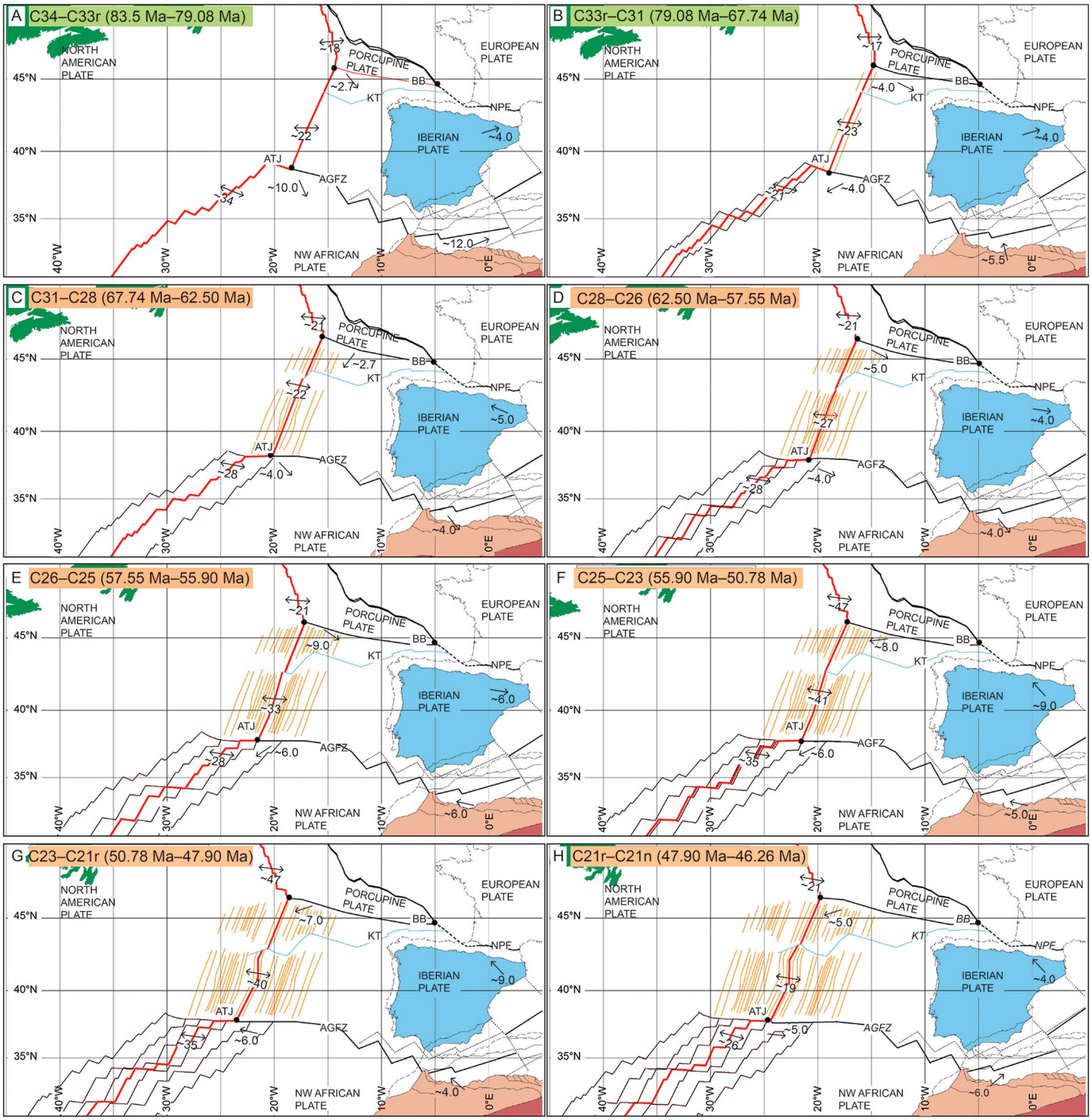

Figure 10. Plate reconstructions at Chrons C34, C33r, C31, C28, C26, C25, C23, and C21r for the southern North Atlantic region, displaying velocity vectors of relative motion along the major plate boundaries. The black dots represent triple junctions. Ocher lines: southern North Atlantic isochrons (this study); red lines: mid-ocean ridges; dark-brown lines: Central Atlantic isochrons (Schettino & Turco, 2011); brown lines: Central Atlantic isochrons (Schettino & Macchiavelli, 2016); dotted lines: inactive boundaries; black lines: active boundaries; pale blue line KT: King's Trough structure; thick black dashed line: hypothetic IB-EU boundary; BB: Bay of Biscay axis; NPF: North Pyrenean Fault; ATJ: Azores Triple Junction; AGFZ: Azores Gibraltar Fracture Zone; black arrows with numbers: relative velocity vectors (velocity in mm yr^{-1}). Present-day coastlines (gray dashed lines) are shown for reference.

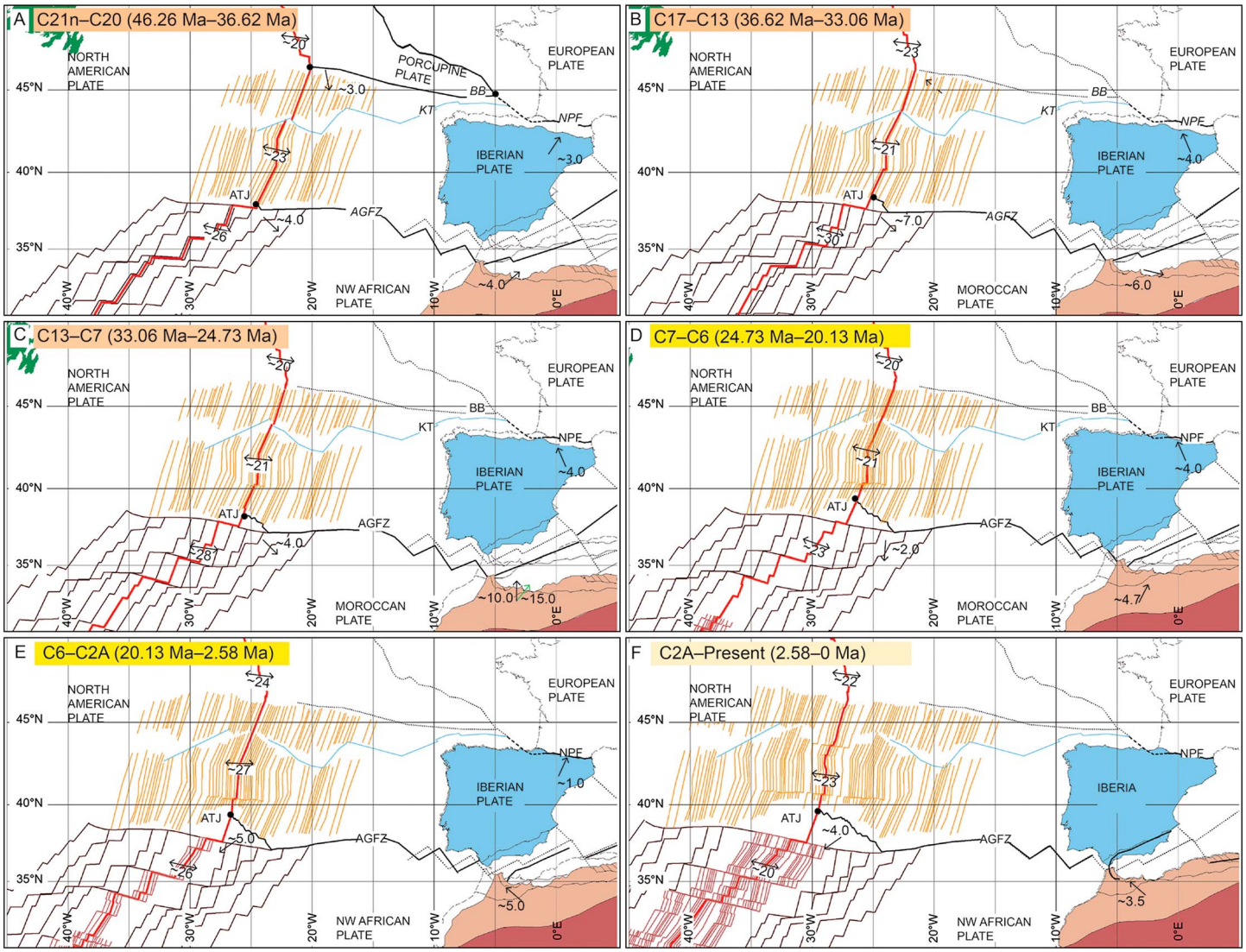

Figure 11. Plate reconstructions at Chrons C21n, C17, C13, C7, C6r, and C2A for the southern North Atlantic region, displaying velocity vectors of relative motion along the major plate boundaries. Green arrow in Figure 11C: Moroccan plate-Iberia velocity vector; other symbols are the same of Figure 10.

NW Africa and Iberia (Figures 10c and 10d). This extension ceased in the Betic domain during the late Thanetian, when the motion became WNW directed (Figure 10e). Along the northern Iberian boundary, the model shows two different phases: (i) SW directed extension along the Bay of Biscay axis while NW directed compression was still affecting the North Pyrenean Fault during the early Paleocene (Figure 10c) and (ii) transtensional movement along the entire Iberia-Europe boundary during the late Paleocene (Figures 10d and 10e). At the Paleocene-Eocene boundary, an increase in spreading rates characterized the Europe-Iberia-North America system (Figure 10f). This event marked the end of the main period of left-lateral motion in the Central Pyrenees. During the late Ypresian (Figure 10g), the model predicts an important change in the kinematics between NW Africa and Iberia: the relative motion between these two plates became NW directed along the entire boundary. As a consequence, the triple junction among NW Africa, Iberia, and North America (the ATJ), which was a stable RRR triple junction until ~50 Ma, became an unstable ridge-fault-thrust triple junction (McKenzie & Morgan, 1969) for several Myr (Figure 10g). This instability resulted in the northward migration of the triple junction. During the Lutetian and Bartonian (Figures 10h and 11a) along the NW Africa-Iberia boundary, our model predicts transtension at the ATJ, sinistral strike-slip movement along the Gloria Fault, and a NNE directed convergent motion in the Betic domain (~6 mm yr^{-1}). At Chron 17 (36.62 Ma, Priabonian), the Iberia-Europe plate boundary jumped from the Bay of Biscay axis to King's Trough

(Figure 11b). This event occurred when the motion along the axis of the Bay of Biscay became mainly strike-slip, and as a consequence, the triple junction among North America, Europe, and Iberia, which was RRR for most of its history, gradually changed to ridge-ridge-fault. This configuration is unstable (McKenzie & Morgan, 1969), and this instability may partly explain the plate boundary shift from the Bay of Biscay axis to King's Trough. The motion across this boundary is completely described by our rotation pole P*, showing overall extension along King's Trough. Starting from Anomaly 17 (~36.62 Ma), the motion across the northern Iberian boundary was accommodated entirely by the King's Trough structure, and NNW directed compression occurred along the North Pyrenean Fault (Figure 11b). Moreover, concurrently with the plate boundary jump, the Porcupine plate started to move with the European plate (Vissers & Meijer, 2012b).

It is worth noting that from Anomaly 15 (34.55 Ma, Priabonian) to Anomaly 6B (22.59 Ma, Aquitanian), the lack of magnetic crossings made the statistical estimation of the Iberia-North America rotation parameters unreliable. Thus, the plate reconstructions for the Priabonian-Aquitanian interval are based on a unique stage pole. However, during the early Oligocene (Chron 13, 33.06 Ma; Figure 11c), our model accounts for the eastward movement of the Moroccan plate with respect to the NW African plate (Schettino & Macchiavelli, 2016). This shift implied an increase in the rate of convergence (average ~15 mm yr^{-1}) in the Betic domain with respect to the "pure" NW Africa-Iberia convergence at an average rate of ~10 mm yr^{-1} until Anomaly 7 (~24.7 Ma, Chattian). At that time, the relative velocity vector between NW Africa and Iberia started to rotate clockwise, becoming S directed at the ATJ, with the NE directed convergence continuing in the Betic domain (Figure 11d). Moreover, during this stage, the opening of the Alboran basin in the inner side of the Betic-Rif orogen occurs. From the early Miocene to the present-day, our model shows a substantial amount of NE-SW directed extension near the Azores and compression along the NW Africa-Iberia plate boundary in the Betic domain. During this period, the main compressional phase along the Pyrenees ceased and was followed by a transpressional phase with slowly increasing rates (Figures 11e and 11f).

5. Discussion

This section is organized to discuss the most significant implications of the presented kinematic model. First, we compare our predicted spreading rates for the southern North Atlantic (Iberia-North America) with the results compiled by Srivastava, Roest, et al. (1990), Srivastava, Schouten, et al. (1990), Rosenbaum et al. (2002), and Vissers and Meijer (2012b) (Figure 8b). Therefore, we discuss the main differences between our model and the previous models in terms of kinematic evolution (Figure 12). Moreover, we explore the geological implication of our model in the Betic-Rif and in the Pyrenees-Bay of Biscay orogenic systems. For this purpose, the predicted N-S convergence rates of NW Africa-Iberia, Iberia-Europe, and NW Africa-Europe have been calculated across the Eastern Betics domain, the Pyrenees-Bay of Biscay, and along a transect in the intervening area, respectively (Figures 13, 14, and S5 in the supporting information). As regarding the present-day kinematics, a comparison with GPS data and the MORVEL (Mid-Ocean Ridge VELocity, DeMets et al., 2010) model is presented. Finally, we investigate the plate driving mechanisms controlling the kinematics presented in the proposed model.

5.1. Southern North Atlantic (Iberia-North America) Spreading Rates

A common trend among the spreading rates predicted by the three previous models and our model can be observed (Figure 8b). This general trend can be summarized in four distinct time intervals with specific values of average spreading rates: (i) an initial period (Late Cretaceous-Paleocene, 83.5–56 Ma) characterized by a spreading rate of ~24 mm yr^{-1}, (ii) a second time interval (Ypresian, 56–48 Ma) with a higher rate (~37 mm yr^{-1}), (iii) a long period of relatively low spreading rate (~21 mm yr^{-1}) from ~48 Ma (Ypresian-Lutetian boundary) to ~20 Ma (Aquitanian-Burdigalian boundary), and (iv) a final increase in the average rate (~25 mm yr^{-1}) from the Aquitanian-Burdigalian boundary (~20 Ma) to present. Our velocity diagram allows these distinct time intervals to be examined in more detail with respect to the previous models. During the first time interval (83.5–56 Ma, Santonian-Campanian boundary to Paleocene-Eocene boundary), our predicted spreading rates are characterized by an average value of ~21 mm yr^{-1} until Chron 28 (62.50 Ma, Danian), except for the time interval between Chrons 34 and 33n (Campanian). At Chron 28 (62.50 Ma, Danian), the velocity progressively increased until the Paleocene-Eocene boundary (~56 Ma). During the second time interval (~56–48 Ma, Paleocene-Eocene boundary to Ypresian), a distinctive event recognized in all the models is a period of high spreading rates during the Ypresian, albeit with substantial differences in terms

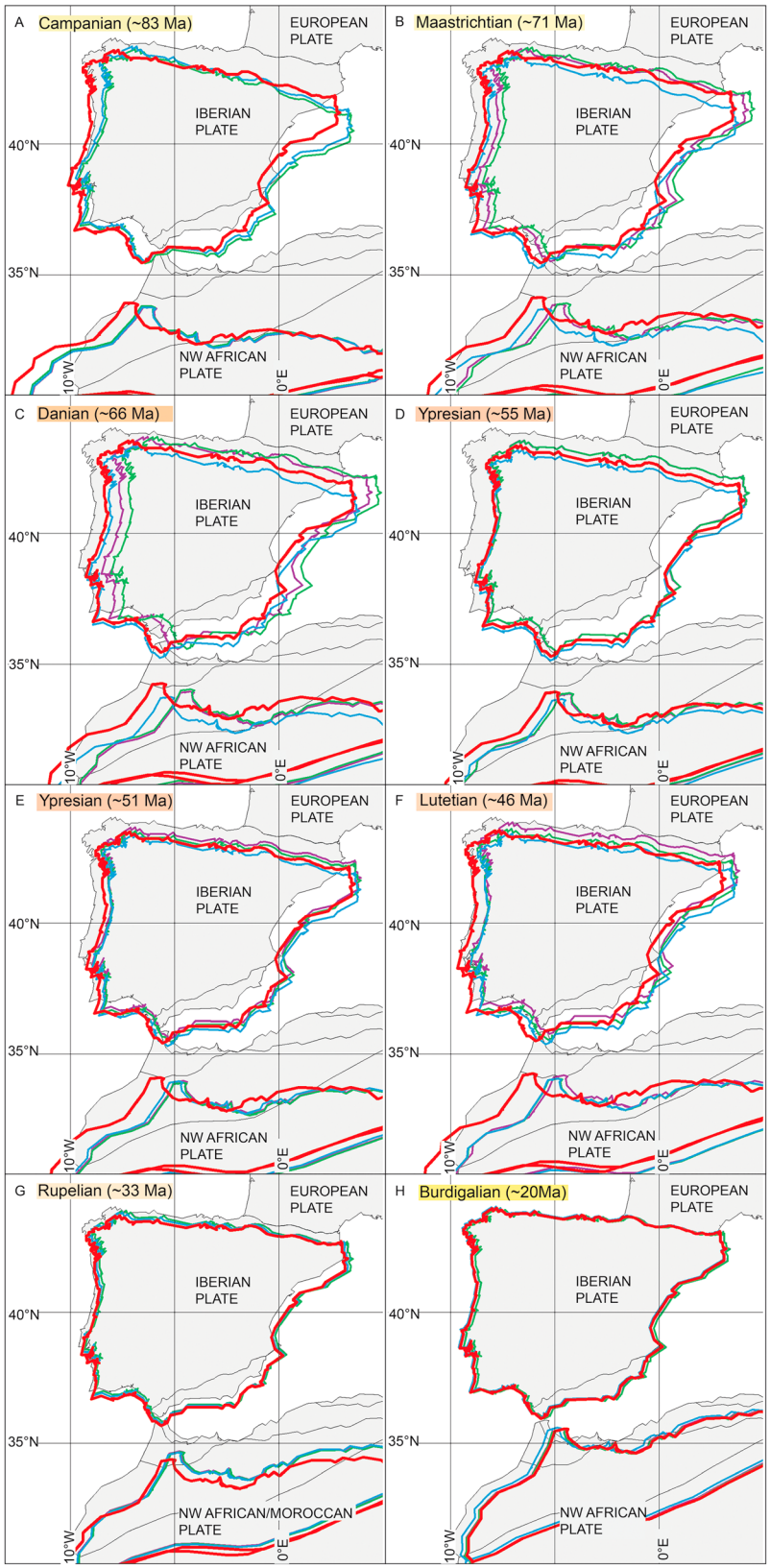

Figure 12. A series of different plate reconstructions for the Iberian and NW African/Moroccan plate. Red line: this work; blue line: Vissers and Meijer (2012b); green line: Rosenbaum et al. (2002); purple line: Srivastava, Roest, et al. (1990). Present-day coastlines (gray areas) are shown for reference.

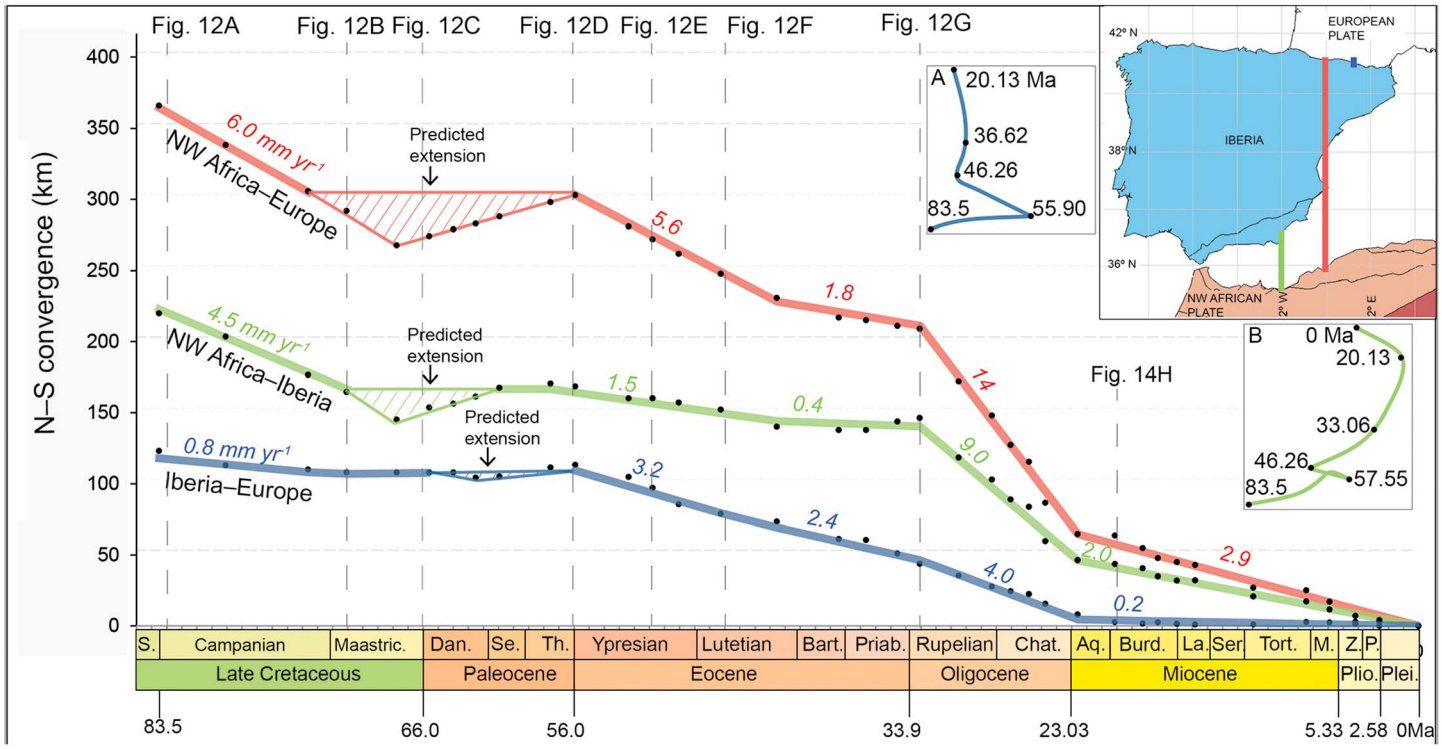

Figure 13. Diagram showing the predicted N-S convergence between NW Africa and Europe (red line), between NW Africa and Iberia in the Betic domain (green line), and between Iberia and Europe in the Pyrenean domain (blue line) since Anomaly 34 (83.5 Ma). The N-S convergence rates are calculated along three different transects (see inset map for locations). Inset A: smoothed Iberia-Europa motion path (Central Pyrenees); Inset B: smoothed NW Africa-Iberia motion path (Eastern Betics).

of maximum velocities among the four different models. In the third time interval (~48 to ~20 Ma, Ypresian-Burdigalian), the three compared models (Rosenbaum et al., 2002; Srivastava, Roest, et al., 1990; Srivastava, Schouten, et al., 1990; Vissers & Meijer, 2012b) predict a transition from ~24 mm yr^{-1} to ~19 mm yr^{-1} around Anomaly 13 (~33 Ma, Eocene-Oligocene boundary). Conversely, in our model, this transition occurred at Chron 17 (36.62 Ma, Priabonian), and the velocity remained constant until Chron 6 (20.13 Ma,

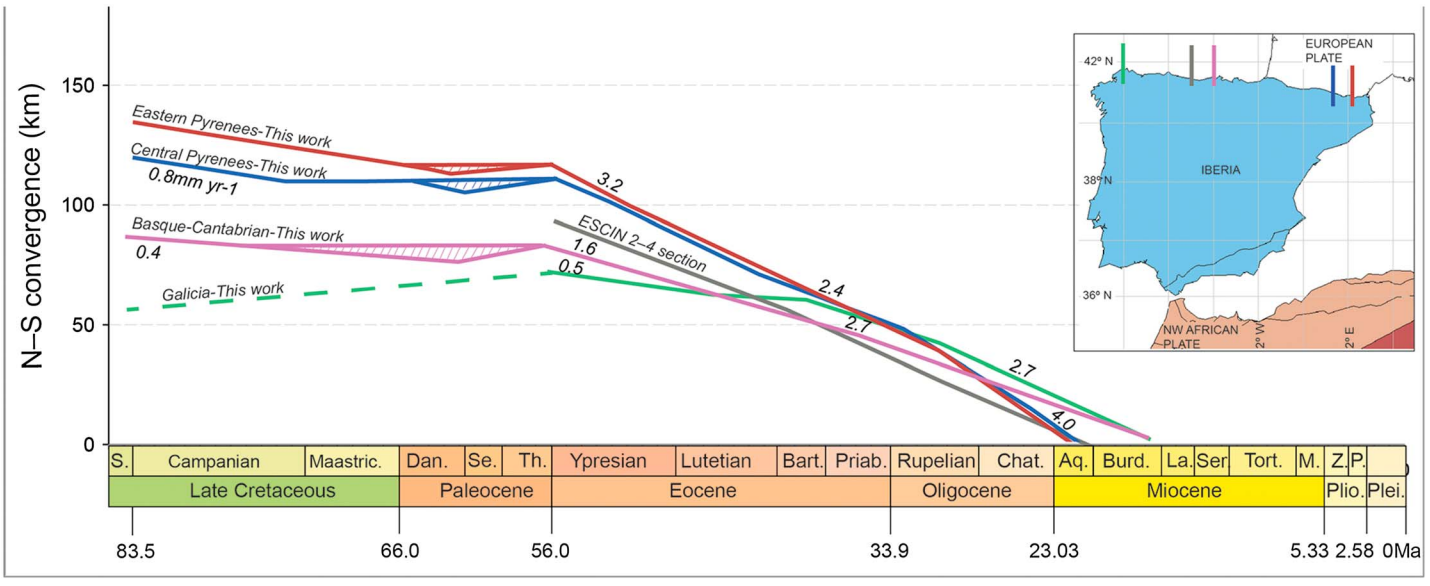

Figure 14. Diagram showing the predicted N-S convergence between Iberia and Europe along four different transect (see inset map for locations). Gray curve: geology data inferred from partially restored sections of Fernández-Viejo and Gallastegui (2005) modified from Vissers and Meijer (2012b).

Burdigalian). Finally, from Chron 6 (20.13 Ma) to the present, our model allows a marked decrease in velocity to be distinguished at Chron 4 (7.43 Ma, Zanclean), which is coeval with a change in the North America-Europe motion detected across the entire North Atlantic (Merkouriev & DeMets, 2008).

5.2. Comparison With Previous Models

The main goal of our model is the reconstruction of the relative position of Iberia through time, as emerged in Figure 12, in which we compare our reconstructions with some recent previous models (Rosenbaum et al., 2002; Srivastava, Roest, et al., 1990; Srivastava, Schouten, et al., 1990; Vissers & Meijer, 2012b). A prominent feature in Figure 12a is the position of the Iberian plate at ~83 Ma (Campanian), which is shifted to the northwest in our kinematic model, as a result of the fitting of the Anomaly 34 crossings (83.5 Ma). A shifting in the Iberian position is also noticeable during the Maastrichtian and Paleocene, although in all models a left-transpressional motion between Iberia and Europe is predicted (Figures 12b and 12c). The four compared models predict almost the same kinematics for the Iberian plate during the Ypresian (Figures 12d and 12e); conversely, our model implies again a shifted position of the Iberian plate during the Lutetian (Figures 12d and 12e). During the Oligocene (33.06–24.73 Ma), our model accounts for the existence of an independent Moroccan plate (Schettino & Macchiavelli, 2016) characterized by dextral strike-slip movement of ~70 km with respect to the NW African plate (Figures 12g and 12h).

5.3. NW Africa-Iberia Plate Boundary

In the model presented in this study, the phase of convergence between Iberia and NW Africa has been active since the Santonian-Campanian boundary (Chron C34, 83.5 Ma). The calculated amount of N-S convergence in the Eastern Betics is ~230 km (Figure 13, green line). A significant part of this amount (~80 km) was accommodated through the Priabonian, followed by additional ~150 km of convergence from the Oligocene onward.

A closer inspection of the N-S convergence velocity curve shows that six different stages can be distinguished. The first stage, from the Santonian-Campanian boundary to the late Maastrichtian, is characterized by a high rate of N-S convergence (~4.5 mm yr^{-1}). During the second stage (late Maastrichtian-early middle Paleocene) our model predicts extension in the Betic domain related to an interruption of significant convergence between Africa and Europe ("Paleocene standstill phase," Schettino & Turco, 2011).

The convergence resumed during late Paleocene and Lutetian (~42 Ma) at a rate of 1.5 mm yr^{-1} (third stage), continuing during the Bartonian and Priabonian at 0.4 mm yr^{-1} (fourth stage). A noticeable increase in the N-S convergence, up to 9 mm yr^{-1}, is predicted from the Oligocene to the earliest Miocene (fifth stage). Subsequently, during the last stage (earliest Miocene to present), the N-S convergence rate slows down to 2 mm yr^{-1}. Our predicted Africa-Iberia N-S convergence rates can be compared with the proposed cumulative shortening Betic-Rif kinematic model by Vergés and Fernàndez (2012) (Figure S5a). It is worth noting that this is only a qualitative comparison to show the roughly good fit of both total shortening and predicted convergence rates. Although the predicted rates appear to be substantially different during the Late Cretaceous-Paleocene-Eocene times, the average rates during this time interval differ for 0.2 mm yr^{-1} and the late Oligocene is characterized by the higher spreading rates (up to ~9 mm yr^{-1}) in both models. Our determinations show that the Africa-Europe convergence (red curve, Figure 13) was initially partitioned across the Pyrenees and the Betic-Rif orogenic system, becoming totally accommodated across the southern margin of Iberia from early Miocene onward.

5.4. Iberia-Europe Plate Boundary

There is a widespread consensus about the fact that the northern Iberia-Europe plate boundary was deformed under a contraction regime from late Santonian until the Miocene, forming the present-day Pyrenees. However, the total amount of shortening, the rates of convergence, and the correspondence between geological and kinematic studies are still matter of debate (Mouthereau et al., 2014, and references therein). Our model predicts a preshortening opening between Iberia and a fixed Europe (~125 km in the N-S direction in the Central Pyrenees; Figure 13, blue curve) smaller with respect to the models of Srivastava, Roest, et al. (1990), Rosenbaum et al. (2002), and Vissers and Meijer (2012b), which implied ~170 km, ~170 km, and ~160 km of separation, respectively. Our predicted value falls in the low range of published shortening estimates across several N-S balanced geological sections (Choukroune & the ECORS-Pyrenees

Team, 1989; Martinez-Peña & Casas-Sainz, 2003; Roure et al., 1989; Teixell, 1998; Vergés et al., 1995). These values of shortening include (i) ~125 km (Vergés et al., 1995) in the Eastern Pyrenees and (ii) ~120 km (Roure et al., 1989), ~147 km (Muñoz, 1992), and ~165 km (Beaumont et al., 2000) in the Central Pyrenees.

Six different stages can be distinguished, albeit with smoothed variations if compared with the NW Africa-Iberia convergence rate curve. The first stage, from the Santonian-Campanian boundary to the Danian-Selandian boundary, is characterized by a slow rate of convergence (~0.8 mm yr^{-1}), which allows to accommodate about 30 km of the total shortening. After a stage of minimum extension (Danian-Selandian boundary to Paleocene-Eocene boundary), the convergence resumed at higher rates during Ypresian-Lutetian (3.2 mm yr^{-1}, third stage), Bartonian-Priabonian (2.4 mm yr^{-1}, fourth stage), and Oligocene times (4.0 mm yr^{-1}, fifth stage). Finally, the shortening rate slows down to 0.2 mm yr^{-1} from the earliest Miocene to present.

From east to west along the Iberia-Europe boundary, our model confirms that the total shortening across the belt tends to decrease toward the west (e.g., Vergés et al., 2002). The convergence is active at the Santonian-Campanian boundary across the Eastern Pyrenees, the Central Pyrenees, and Basque-Cantabrian margin, while it is younger in Galicia shifting at Paleocene-Eocene boundary (Figure 14). Along the Basque-Cantabrian margin, N-S convergence at low rates is predicted from the Santonian-Campanian boundary to the Paleocene-Eocene boundary, followed by a rapid increase in convergence rate (1.6 mm yr^{-1}), characterized by the accommodation of ~85 km of convergence in N-S direction until the middle Miocene (Figure 14). The timing along the Basque-Cantabrian margin is in agreement with the deformation history proposed by Roca et al. (2011), Ferrer et al. (2012), and Tugend, Manatschal, and Kusznir (2015), in which the first compressional event in this domain is recorded in late Santonian-Campanian times. Moreover, a comparison between our N-S convergence rates and the shortening inferred from the partial restoration of the ESCIN section (Vissers & Meijer, 2012b modified from Fernández-Viejo & Gallastegui, 2005) shows a substantial correspondence in terms of convergence rates as indicated by the sudden increase of the tectonic subsidence rate at ~54 Ma (Gómez et al., 2002).

Conversely, across the Galician coast, our model predicts extensional kinematics during the Late Cretaceous and Paleocene, followed by a compressional event from the Ypresian (Figure 14). The predicted Late Cretaceous-Paleocene transtension is difficult to account in the current geological model (Tugend et al., 2015, 2014, and references therein). In the Eastern and Central Pyrenees, the shortening ends in the late Aquitanian, whereas in the Basque-Cantabrian Basin and Galicia ends in the late Burdigalian (Figure 14). To test our kinematic model in the Pyrenees domain, we compare our shortening estimates for the Eastern and Central Pyrenees with shortening rates derived from balanced and restored geological sections and well-calibrated ages for associated growth strata calculated by Vergés et al. (1995) for the Eastern Pyrenees (Figure S5b) and by Beaumont et al. (2000) and Mouthereau et al. (2014) for the Central Pyrenees (Figure S5c).

Our proposed reconstruction fits well with the shortening inferred from the balanced cross section in the Eastern Pyrenees of Vergés et al. (1995), which determined an initially slow convergence of Iberia, increasing from the early Eocene onward (Figure S5b). The predicted deformation histories become rather different only during the middle Eocene. Vergés et al. (1995) identified a distinct stage (from 47 Ma to the early Priabonian, which was near the top of the preserved growth strata), in which the rate considerably slows down. Our model, however, predicts a quite regular trend at higher rate (Figure S5b).

The comparison between our results and the shortening rates compiled by Mouthereau et al. (2014) and modeled by Beaumont et al. (2000) in the Central Pyrenees (Figure S5c) shows a substantial difference in terms of total shortening, with a total difference of about 50 km lower in our model. Moreover, our rates are considerably lower during Late Cretaceous-Paleocene times, in particular when compared with the results of Mouthereau et al. (2014), which identify the most rapid shortening rates at the onset of convergence at 80–60 Ma followed by a long period characterized by a constant rate of ~2.0 mm yr^{-1}. On the contrary, there is a good agreement between our model and the model of Beaumont et al. (2000), as both assume the highest shortening rates after 34 Ma.

5.5. Present-Day Kinematics

Regarding the present-day kinematics, we compared our results for Anomaly 2A with the 3 Myr average MORVEL (Mid-Ocean Ridge VELocity, DeMets et al., 2010) Europe-North America pole (Figure 8a). The angular

distance between our 2A rotation pole and the MORVEL pole is ~5.2°. An inspection of the present-day relative velocity vector between Africa and Iberia along the AGFZ shows that our model implies a substantial amount of extension near the Azores and a large amount of compression along the plate boundary between Africa and Iberia in the Betic domain. This is in agreement with both the observed extension at the ATJ (Marques et al., 2013) and the compression between Africa and Iberia as reflected in the Betic-Rif orogenic system. In support, recent GPS data determinations (Marques et al., 2013) show that the ATJ spreading rates decrease gradually from ~22.5 mm yr^{-1} north of 40°N to 19.5 mm yr^{-1} south of 38°N, which is in good agreement with our results implying a spreading rate of ~23–23.5 mm yr^{-1} north of 40°N and of ~20.5 mm yr^{-1} south of 38°N.

5.6. Plate Driving Mechanisms

The main forces acting upon tectonic plates are ridge push, slab pull, and mantle drag, whereas ridge push and slab pull are associated with the generation and subduction of oceanic lithosphere, respectively; mantle drag is related to sublithospheric mantle flow. North-south convergence between Africa and Eurasia initiated during the Late Cretaceous mostly driven by the combined push of the south-Atlantic and South Indian ridges together with the intraoceanic northeast dipping subduction of the Tethyan lithosphere in North Africa (Gaina et al., 2013). The convergence between Africa and Eurasia continued until recent producing the complete consumption of the westernmost Alpine-Tethys oceanic domain, intraplate deformation in Iberia, and incipient subduction along its northern margin. The inherited Jurassic segmentation of the Alpine-Tethys domain allowed for opposed subduction polarities in adjacent plate segments during its consummation. Consequently, the present back arc Western Mediterranean basins formed as a combination of ridge push driving the northern displacement of Africa, slab pull driving the retreating of the Alpine-Tethys subducting slabs in different directions, and the mantle drag generated by the return flow of these retreating slabs together with the body forces associated with lateral density variations in the sublithospheric mantle (e.g., Casciello et al., 2015; Faccenna et al., 2014; Mériaux et al., 2015; Neres et al., 2016).

6. Concluding Remarks

1. A new methodology to obtain 37 reliable Euler rotation poles in the southern North Atlantic region since the Late Cretaceous (83.5 Ma) has been proposed, overcoming the absence of well-defined fracture zones and transform faults.
2. The evolution of the drift of the Iberian plate has been described through 14 different steps, reconstructing the detailed kinematics across its northern and southern boundaries. Our determinations have confirmed that the motion along the Iberia-Europe boundary occurred along the Bay of Biscay axis from the Santonian-Campanian boundary to the middle Priabonian, before jumping to the King's Trough at Anomaly 17 (36.62 Ma, Priabonian).
3. Compared with previous models, the Iberian plate was shifted to the west from the Santonian-Campanian boundary to early Paleocene and during the Lutetian. On the other hand, there is a good agreement at the large scale among the different models during the other evolutionary stages.
4. The seafloor spreading history between Iberia and North America since 83.5 Ma has been described through four distinct time intervals with specific values of average spreading rates. However, we have shown that at least 10 substages can be detailed.
5. The convergence of NW Africa with respect to Iberia in the Eastern Betics domain was already active at the Santonian-Campanian boundary (Chron C34, 83.5 Ma), accommodating at least 80 km of convergence until the early Oligocene. Accordingly, the shortening related to the Africa-Europe convergence is partitioned between the northern and southern boundary of the Iberian plate, and the Azores Gibraltar Fracture Zone constituted an active plate boundary between Iberia and Africa already from the Late Cretaceous. Six different stages have been distinguished in the NW Africa- Iberia N-S convergence velocity curve.
6. In the Central Pyrenees, the total predicted amount of N-S shortening is ~125 km, in the low range of published shortening estimates. Six different stages can be distinguished, with the higher convergence rates documented during the Eocene and Oligocene. The convergence was active at the Santonian-Campanian boundary across the Eastern Pyrenees, the Central Pyrenees, and Basque-Cantabrian margin, while it started at Paleocene-Eocene boundary in Galicia.
7. The present-day kinematics along the Azores Gibraltar Fracture Zone implies NE-SW directed extension near the Azores Triple Junction and NNE directed convergent motion in the Betic domain.

Acknowledgments
The present work has been supported by ALPIMED (PIE-CSIC-201530E082) project. The ship-track and aeromagnetic track data analyzed in this work are available online from https://maps.ngdc.noaa.gov/viewers/geophysics/. The marine magnetic anomaly analysis software was designed by A. Schettino and is available from http://www.serg.unicam.it/Downloads.htm. The reconstructions in this paper were created using PCME and GPlates software. We thank J.C. Duarte, M. Nirrengarten, and the Associate Editor for their constructive criticism and suggestions, which considerably improved the quality of the manuscript.

References

Barnett-Moore, N., Hosseinpour, M., & Maus, S. (2016). Assessing discrepancies between previous plate kinematic models of Mesozoic Iberia and their constraints. *Tectonics*, *35*, 1843–1862. https://doi.org/10.1002/2015TC004019

Beaumont, C., Muñoz, J. A., Hamilton, J., & Fullsack, P. (2000). Factors controlling the Alpine evolution of the central Pyrenees inferred from a comparison of observations and geodynamical models. *Journal of Geophysical Research*, *105*(B4), 8121–8145. https://doi.org/10.1029/1999JB900390

Bronner, A., Sauter, D., Manatschal, G., Péron-Pinvidic, G., & Munschy, M. (2011). Magmatic breakup as an explanation for magnetic anomalies at magma-poor rifted margins. *Nature Geoscience*, *4*(8), 549–553. https://doi.org/10.1038/ngeo1201

Cande, S. C., & Kent, D. V. (1995). Revised calibration of the geomagnetic polarity timescale for the Late Cretaceous and Cenozoic. *Journal of Geophysical Research*, *100*(B4), 6093–6095. https://doi.org/10.1029/94JB03098

Canérot, J. (2016). The Iberian Plate: Myth or reality? *Boletín Geológico y Minero*, *127*(2), 563–574.

Casciello, E., Fernàndez, M., Vergés, J., Cesarano, M., & Torne, M. (2015). The Alboran domain in the western Mediterranean evolution: The birth of a concept. *Bulletin de la Societe Geologique de France*, *186*(4-5), 371–384. https://doi.org/10.2113/gssgfbull.186.4-5.371

Choukroune, P., & the ECORS-Pyrenees Team (1989). The ECORS-Pyrenean deep seismic profile reflection data and the overall structure of the orogenic belt. *Tectonics*, *8*(1), 23–39. https://doi.org/10.1029/TC008i001p00023

Chu, D., & Gordon, R. G. (1998). Current plate motions across the Red Sea. *Geophysical Journal International*, *135*(2), 313–328. https://doi.org/10.1046/j.1365-246X.1998.00658.x

DeMets, C., Gordon, R. G., & Argus, D. F. (2010). Geologically current plate motions. *Geophysical Journal International*, *181*(1), 1–80. https://doi.org/10.1111/j.1365-246X.2009.04491.x

DeMets, C., Iaffaldano, G., & Merkouriev, S. (2015). High-resolution Neogene and Quaternary estimates of Nubia–Eurasia–North America Plate motion. *Geophysical Journal International*, *203*(1), 416–427. https://doi.org/10.1093/gji/ggv277

DeMets, C., & Wilson, D. S. (2008). Toward a minimum change model for recent plate motions: Calibrating seafloor spreading rates for outward displacement. *Geophysical Journal International*, *174*(3), 825–841. https://doi.org/10.1111/j.1365-246X.2008.03836.x

Deverchere, J., Yelles, K., Domzig, A., Mercier de Lépinay, B., Bouillin, J. P., Gaullier, V., … Dan, G. (2005). Active thrust faulting offshore Boumerdes, Algeria, and its relations to the 2003 M_w 6.9 earthquake. *Geophysical Research Letters*, *32*, L04311. https://doi.org/10.1029/2004GL021646

Eddy, M. P., Oliver, J., & Ibañez-Mejia, M. (2017). Timing of initial seafloor spreading in the Newfoundland–Iberia rift. *Geology*, *45*(6), 527–530. https://doi.org/10.1130/G38766.1

Faccenna, C., Becker, T. W., Auer, L., Billi, A., Boschi, L., Brun, J. P., … Serpelloni, E. (2014). Mantle dynamics in the Mediterranean. *Reviews of Geophysics*, *52*, 283–332. https://doi.org/10.1002/1013RG000444

Fernández-Viejo, G., & Gallastegui, J. (2005). The ESCI-N project after a decade: A synthesis of the results and open questions. *Trabajos de Geología, Universidad de Oviedo*, *25*, 9–25.

Ferrer, O., Jackson, M. P. A., Roca, E., & Rubinat, M. (2012). Evolution of salt structures during extension and inversion of the Offshore Parentis Basin (Eastern Bay of Biscay). *Geological Society of London, Special Publication*, *363*(1), 361–380. https://doi.org/10.1144/SP363.16

Frizon de Lamotte, D., Raulin, C., Mouchot, N., Wrobel-Daveau, J. C., Blanpied, C., & Ringenbach, J. C. (2011). The southernmost margin of the Tethys realm during the Mesozoic and Cenozoic: Initial geometry and timing of the inversion processes. *Tectonics*, *30*, TC3002. https://doi.org/10.1029/2010TC002691

Gaina, C., Torsvik, T. H., van Hinsbergen, D. J., Medvedev, S., Werner, S. C., & Labails, C. (2013). The African Plate: A history of oceanic crust accretion and subduction since the Jurassic. *Tectonophysics*, *604*, 4–25. https://doi.org/10.1016/j.tecto.2013.05.037

Gómez, M., Vergés, J., & Riaza, C. (2002). Inversion tectonics of the northern margin of the Basque Cantabrian Basin. *Bulletin de la Societe Geologique de France*, *173*(5), 449–459. https://doi.org/10.2113/173.5.449

Handy, M. R., Schmid, S. M., Bousquet, R., Kissling, E., & Bernoulli, D. (2010). Reconciling plate-tectonic reconstructions of Alpine Tethys with the geological–geophysical record of spreading and subduction in the Alps. *Earth-Science Reviews*, *102*(3-4), 121–158. https://doi.org/10.1016/j.earscirev.2010.06.002

Hellinger, S. J. (1981). The uncertainties of finite rotations in plate tectonics. *Journal of Geophysical Research*, *86*(B10), 9312–9318. https://doi.org/10.1029/JB086iB10p09312

Jammes, S., Manatschal, G., Lavier, L., & Masini, E. (2009). Tectonosedimentary evolution related to extreme crustal thinning ahead of a propagating ocean: Example of the western Pyrenees. *Tectonics*, *28*, TC4012. https://doi.org/10.1029/2008TC002406

Kerr, J. W., Fergusson, A. J., & Machan, L. C. (1981). *Geology of the North Atlantic borderlands*. Calgary, Canada: Canadian Society of Petroleum Geologists.

Klitgord, K., & Schouten, H. (1986). Plate kinematics of the central Atlantic, The Geology of North America: The Western Atlantic Region, DNAG Ser. M PR Vogt, BE Tucholke: 351–378.

Le Pichon, X., & Sibuet, J. C. (1971). Western extension of boundary between European and Iberian plates during the Pyrenean orogeny. *Earth and Planetary Science Letters*, *12*(1), 83–88. https://doi.org/10.1016/0012-821X(71)90058-6

Marques, F. O., Catalão, J. C., DeMets, C., Costa, A. C. G., & Hildenbrand, A. (2013). GPS and tectonic evidence for a diffuse plate boundary at the Azores Triple Junction. *Earth and Planetary Science Letters*, *381*, 177–187. https://doi.org/10.1016/j.epsl.2013.08.051

Martinez-Peña, M., & Casas-Sainz, A. (2003). Cretaceous–Tertiary tectonic inversion of the Cotiella Basin (southern Pyrenees, Spain). *International Journal of Earth Sciences (Geologische Rundschau)*, *92*(1), 99–113. https://doi.org/10.1007/s00531-002-0283-x

Matias, L. M., Olivet, J. L., Aslanian, D., & Fidalgo, L. (2005). PLACA: A white box for plate reconstruction and best-fit pole determination. *Computers and Geosciences*, *31*(4), 437–452. https://doi.org/10.1016/j.cageo.2004.09.019

McKenzie, D. P., & Morgan, W. J. (1969). Evolution of triple junctions. *Nature*, *224*(5215), 125–133. https://doi.org/10.1038/224125a0

Mériaux, C. A., Duarte, J. C., Duarte, S. S., Schellart, W. P., Chen, Z., Rosas, F., … Terrinha, P. (2015). Capture of the Canary mantle plume material by the Gibraltar arc mantle wedge during slab rollback. *Geophysical Journal International*, *201*(3), 1717–1721. https://doi.org/10.1093/gji/ggv120

Merkouriev, S., & DeMets, C. (2006). Constraints on Indian plate motion since 20 Ma from dense Russian magnetic data: Implications for Indian plate dynamics. *Geochemistry, Geophysics, Geosystems*, *7*, Q02002. https://doi.org/10.1029/2005GC001079

Merkouriev, S., & DeMets, C. (2008). A high-resolution model for Eurasia–North America plate kinematics since 20 Ma. *Geophysical Journal International*, *173*(3), 1064–1083. https://doi.org/10.1111/j.1365-246X.2008.03761.x

Merkouriev, S., & DeMets, C. (2014a). High-resolution Neogene reconstructions of Eurasia–North America Plate motion. *Geophysical Journal International*, *198*(1), 366–384. https://doi.org/10.1093/gji/ggu142

Merkouriev, S., & DeMets, C. (2014b). High-resolution estimates of Nubia–North America plate motion: 20 Ma to present. *Geophysical Journal International*, *196*(3), 1281–1298. https://doi.org/10.1093/gji/ggt463

Miles, P. R., & Kidd, R. B. (1986). Correlation of seafloor spreading magnetic anomalies across King's Trough, Northeast Atlantic. In *Initial Reports DSDP* (Vol. 94, pp. 1149–1156). Washington, DC: U.S. Government Printing Office.

Mouthereau, F., Filleaudeau, P. Y., Vacherat, A., Pik, R., Lacombe, O., Fellin, M. G., … Masini, E. (2014). Placing limits to shortening evolution in the Pyrenees: Role of margin architecture and implications for the Iberia/Europe convergence. *Tectonics*, *33*, 2283–2314. https://doi.org/10.1002/2014TC003663

Müller, R. D., & Roest, W. R. (1992). Fracture zones in the North Atlantic from combined Geosat and Seasat data. *Journal of Geophysical Research*, *97*(B3), 3337–3350. https://doi.org/10.1029/91JB02605

Müller, R. D., Roest, W. R., Royer, J.-Y., Gahagan, L. M., & Sclater, J. G. (1997). Digital isochrons of the world's ocean floor. *Journal of Geophysical Research*, *102*(B2), 3211–3214. https://doi.org/10.1029/96JB01781

Müller, R. D., Sandwell, D. T., Tucholke, B. E., Sclater, J. G., & Shaw, P. R. (1990). Depth to basement and geoid expression in the Kane Fracture Zone: A comparison. *Marine Geophysical Researches*, *13*, 105–129.

Müller, R. D., Seton, M., Zahirovic, S., Williams, S. E., Matthews, K. J., Wright, N. M., … Cannon, J. (2016). Ocean basin evolution and global-scale plate reorganization events since Pangea breakup. *Annual Review of Earth and Planetary Sciences*, *44*(1), 107–138. https://doi.org/10.1146/annurev-earth-060115-012211

Muñoz, J. A. E. (1992). Evolution of a continental collision belt: ECORS-Pyrenees crustal balanced cross-section. In K. McClay (Ed.), *Thrust Tectonics* (pp. 235–246). London: Chapman and Hall. https://doi.org/10.1007/978-94-011-3066-0_21

Neres, M., Carafa, M. M. C., Fernandes, R. M. S., Matias, L., Duarte, J. C., Barba, S., & Terrinha, P. (2016). Lithospheric deformation in the Africa-Iberia plate boundary: Improved neotectonic modeling testing a basal-driven Alboran plate. *Journal of Geophysical Research: Solid Earth*, *121*, 6566–6596. https://doi.org/10.1002/2016JB013012

Nirrengarten, M., Manatschal, G., Tugend, J., Kusznir, N. J., & Sauter, D. (2017). Nature and origin of the J magnetic anomaly offshore Iberia–Newfoundland: Implications for plate reconstructions. *Terra Nova*, *29*(1), 20–28. https://doi.org/10.1111/ter.12240

Norton, I., Lawver, L., & Gahagan, L. (2007). Plate motion of Iberia relative to Europe in the Cretaceous: Problems with the fit at M0 time, AGU Fall Meeting Abstracts, 08.

Olivet, J. L. (1996). La cinématique de la plaque Ibérique. *Bulletin des Centres de Recherches Exploration-Production Elf-Aquitaine*, *20*, 131–195.

Olivet, J. L., Bonnin, J., Beuzart, P., & Auzende, J. M. (1984). Cinématique de l'Atlantique nord et central: Brest, Centre National pour l'Exploitation des Océans, Rapports scientifiques and techniques 54,108 pp.

Péron-Pinvidic, G., & Manatschal, G. (2009). The final rifting evolution at deep magma-poor passive margins: A new point of view based on observations from Iberia-Newfoundland. *International Journal of Earth Sciences*, *98*, 7.

Péron-Pinvidic, G., Manatschal, G., Minshull, T., & Sawyer, D. (2007). Tectonosedimentary evolution of the deep Iberia-Newfoundland margins: Evidence for a complex breakup history. *Tectonics*, *26*, TC2011. https://doi.org/10.1029/2006TC001970

Roca, E., Muñoz, J. A., Ferrer, O., & Ellouz, N. (2011). The role of the Bay of Biscay Mesozoic extensional structure in the configuration of the Pyrenean orogen: Constraints from the MARCONI deep seismic reflection survey. *Tectonics*, *30*, TC2001. https://doi.org/10.1029/2010TC002735

Roest, W. R., & Srivastava, S. P. (1991). Kinematics of the plate boundaries between Eurasia, Iberia, and Africa in the North Atlantic from the Late Cretaceous to the present. *Geology*, *19*(6), 613–616. https://doi.org/10.1130/0091-7613(1991)019%3C0613:KOTPBB%3E2.3.CO;2

Rosenbaum, G., Lister, G. S., & Duboz, C. (2002). Relative motions of Africa, Iberia and Europe during Alpine orogeny. *Tectonophysics*, *359*(1-2), 117–129. https://doi.org/10.1016/S0040-1951(02)00442-0

Roure, F., Choukroune, P., Beràstegui, X., Muñoz, J. A., Villien, A., Matheron, P., … Déramond, J. (1989). ECORS deep seismic data and balanced cross sections: Geometric constraints on the evolution of the Pyrenees. *Tectonics*, *8*(1), 41–50. https://doi.org/10.1029/TC008i001p00041

Rowley, D. B., & Lottes, A. L. (1988). Plate-kinematic reconstructions of the North Atlantic and Arctic: Late Jurassic to present. *Tectonophysics*, *155*(1-4), 73–120. https://doi.org/10.1016/0040-1951(88)90261-2

Russell, S. M., & Whitmarsh, R. B. (2003). Magmatism at the west Iberia non-volcanic rifted continental margin: Evidence from analyses of magnetic anomalies. *Geophysical Journal International*, *154*(3), 706–730. https://doi.org/10.1046/j.1365-246X.2003.01999.x

Sallarès, V., Gailler, A., Gutscher, M. A., Graindorge, D., Bartolomé, R., Gracia, R., … Zitellini, N. (2011). Seismic evidence for the presence of Jurassic oceanic crust in the central Gulf of Cadiz (SW Iberian margin). *Earth and Planetary Science Letters*, *311*(1-2), 112–123. https://doi.org/10.1016/j.epsl.2011.09.003

Schettino, A. (2012). Magan: A new approach to the analysis and interpretation of marine magnetic anomalies. *Computers and Geosciences*, *39*, 135–144. https://doi.org/10.1016/j.cageo.2011.07.007

Schettino, A. (2014). *Quantitative plate tectonics: Physics of the Earth–plate kinematics–geodynamics*. New York, NY: Springer.

Schettino, A., & Macchiavelli, C. (2016). Plate kinematics of the central Atlantic during the Oligocene and early Miocene. *Geophysical Journal International*, *205*(1), 408–426. https://doi.org/10.1093/gji/ggw022

Schettino, A., Macchiavelli, C., Pierantoni, P. P., Zanoni, D., & Rasul, N. (2016). Recent kinematics of the tectonic plates surrounding the Red Sea and Gulf of Aden. *Geophysical Journal International*, *207*(1), 457–480. https://doi.org/10.1093/gji/ggw280

Schettino, A., & Scotese, C. R. (2005). Apparent polar wander paths for the major continents (200 Ma to the present day): A palaeomagnetic reference frame for global plate tectonic reconstructions. *Geophysical Journal International*, *163*(2), 727–759. https://doi.org/10.1111/j.1365-246X.2005.02638.x

Schettino, A., & Turco, E. (2011). Tectonic history of the western Tethys since the Late Triassic. *Bulletin Geological Society of America*, *123*(1-2), 89–105. https://doi.org/10.1130/B30064.1

Sibuet, J. C., & Collette, B. J. (1991). Triple junctions of Bay of Biscay and North Atlantic: New constraints on the kinematic evolution. *Geology*, *19*(5), 522–525. https://doi.org/10.1130/0091-7613(1991)019%3C0522:TJOBOB%3E2.3.CO;2

Sibuet, J. C., Monti, S., Lobrieu, B., Mazé, J. P., & Srivastava, S. P. (2004). Carte bathymétrique de l'Atlantique nord-est et du golfe de Gascogne: implications cinématiques. *Bulletin de la Societe Geologique de France*, *175*(5), 429–442. https://doi.org/10.2113/175.5.429

Sibuet, J. C., Srivastava, S. P., & Manatschal, G. (2007). Exhumed mantle-forming transitional crust in the Newfoundland–Iberia rift and associated magnetic anomalies. *Journal of Geophysical Research*, *112*, B06105. https://doi.org/10.1029/2005JB003856

Sibuet, J. C., Srivastava, S. P., & Spakman, W. (2004). Pyrenean orogeny and plate kinematics. *Journal of Geophysical Research*, *109*, B08104. https://doi.org/10.1029/2003JB002514

Srivastava, S. P., & Roest, W. R. (1989). Seafloor spreading history II–IV. In *East Coast Basin Atlas Series:* Labrador Sea, (Map sheets L17–2 - L17–6, pp. 100–109), Atlantic Geoscience Centre, Geologic Survey of Canada, Dartmouth, NS.

Srivastava, S. P., & Roest, W. R. (1992). King's Trough: Reactivated pseudo-fault of a propagating rift. *Geophysical Journal International*, *108*(1), 143–150. https://doi.org/10.1111/j.1365-246X.1992.tb00845.x

Srivastava, S. P., & Roest, W. R. (1996). Porcupine plate hypothesis: Comment. *Marine Geophysical Researches*, *18*(5), 589–593. https://doi.org/10.1007/BF00310070

Srivastava, S. P., Roest, W. R., Kovacs, L. C., Oakey, G., Levesque, S., Verhoef, J., & Macnab, R. (1990). Motion of Iberia since the Late Jurassic: Results from detailed aeromagnetic measurements in the Newfoundland Basin. *Tectonophysics*, *184*(3-4), 229–260. https://doi.org/10.1016/0040-1951(90)90442-B

Srivastava, S. P., Schouten, H., Roest, W. R., Klitgord, K. D., & Kovacs, L. C. (1990). Iberian plate kinematics: A jumping plate boundary between Eurasia and Africa. *Nature*, *344*(6268), 756–759. https://doi.org/10.1038/344756a0

Srivastava, S. P., Sibuet, J. C., Cande, S., Roest, W. R., & Reid, I. D. (2000). Magnetic evidence for slow seafloor spreading during the formation of the Newfoundland and Iberian margins. *Earth and Planetary Science Letters*, *182*(1), 61–76. https://doi.org/10.1016/S0012-821X(00)00231-4

Srivastava, S. P., & Tapscott, C. (1986). Plate kinematics of the North Atlantic. *The Geology of North America*, *1000*, 379–404.

Stampfli, G., Borel, G., Marchant, R., & Mosar, J. (2002). Western Alps geological constraints on western Tethyan reconstructions. *Journal of the Virtual Explorer*, *8*, 77–106.

Teixell, A. (1998). Crustal structure and orogenic material budget in the west central Pyrenees. *Tectonics*, *17*(3), 395–406. https://doi.org/10.1029/98TC00561

Torsvik, T. H., Van der Voo, R., Meert, J. G., Mosar, J., & Walderhaug, H. J. (2001). Reconstructions of the continents around the North Atlantic at about the 60th parallel. *Earth and Planetary Science Letters*, *187*(1-2), 55–69. https://doi.org/10.1016/S0012-821X(01)00284-9

Tucholke, B. E., Sawyer, D. S., & Sibuet, J. C. (2007). Breakup of the Newfoundland–Iberia rift. *Geological Society of London, Special Publication*, *282*(1), 9–46. https://doi.org/10.1144/SP282.2

Tugend, J., Manatschal, G., & Kusznir, N. J. (2015). Spatial and temporal evolution of hyperextended rift systems: Implication for the nature, kinematics, and timing of the Iberian-European plate boundary. *Geology*, *43*(1), 15–18. https://doi.org/10.1130/G36072.1

Tugend, J., Manatschal, G., Kusznir, N. J., Masini, E., Mohn, G., & Thinon, I. (2014). Formation and deformation of hyperextended rift systems: Insights from rift domain mapping in the Bay of Biscay-Pyrenees. *Tectonics*, *33*, 1239–1276. https://doi.org/10.1002/2014TC003529

Vergés, J., & Fernàndez, M. (2012). Tethys–Atlantic interaction along the Iberia–Africa plate boundary: The Betic–Rif orogenic system. *Tectonophysics*, *579*, 144–172. https://doi.org/10.1016/j.tecto.2012.08.032

Vergés, J., Fernàndez, M., & Martìnez, A. (2002). The Pyrenean orogen: Pre-, syn-, and post-collisional evolution. *Journal of the Virtual Explorer*, *8*, 55–74.

Vergés, J., Millan, H., Roca, E., Muñioz, J. A., & Marzo, M. (1995). Eastern Pyrenees and related foreland basins: Pre-, syn-and post-collisional crustal-scale cross-sections. *Marine and Petroleum Geology*, *12*(8), 903–915. https://doi.org/10.1016/0264-8172(95)98854-X

Verhoef, J., Roest, W. R., Macnab, R., & Arkani-Hamed, J. (1996). Members of the project team, magnetic anomalies of the Arctic and North Atlantic Oceans and adjacent land areas, Open File 3125. Geological Survey of Canada. Von Rad U., Sarti M. 1986. Early Cretaceous events in the evolution of the eastern and western North Atlantic continental margins. *Geologische Rundschau*, *75*(1), 139–158.

Vissers, R. L. M., & Meijer, P. T. (2012a). Mesozoic rotation of Iberia: Subduction in the Pyrenees? *Earth-Science Reviews*, *110*(1-4), 93–110. https://doi.org/10.1016/j.earscirev.2011.11.001

Vissers, R. L. M., & Meijer, P. T. (2012b). Iberian plate kinematics and Alpine collision in the Pyrenees. *Earth-Science Reviews*, *114*(1-2), 61–83. https://doi.org/10.1016/j.earscirev.2012.05.001

Vogt, P. R. (1986). *The Western North Atlantic Region* (Vol. 1, pp. 189–204). Boulder, CO: Geological Society of America.

Whitmarsh, R. B., & Miles, P. R. (1995). Models of the development of the West Iberia rifted continental margin at 40°30′N deduced from surface and deep-tow magnetic anomalies. *Journal of Geophysical Research*, *100*(B3), 3789–3806. https://doi.org/10.1029/94JB02877

Zitellini, N., Gràcia, E., Matias, L., Terrinha, P., Abreu, M. A., DeAlteriis, G., … Diez, S. (2009). The quest for the Africa–Eurasia plate boundary west of the Strait of Gibraltar. *Earth and Planetary Science Letters*, *280*(1-4), 13–50. https://doi.org/10.1016/j.epsl.2008.12.005